

Metastability and dynamics in remanent states of square artificial spin ice with long-range dipole interactions

G. M. Wysin*

Department of Physics, Kansas State University, Manhattan, KS 66506-2601

(Dated: 18 October 2023)

After removal of an applied magnetic field, artificial square spin ice can be left in a metastable remanent state, with nonzero residual magnetization and excess energy above the ground state. Using a model of magnetic islands with dipoles of fixed magnitude and local anisotropies, the remanent states are precisely determined here, including all long-range dipole interactions. Small deviations away from remanent states are analyzed and the frequencies of modes of oscillation are determined. Some modes reach zero frequency at high symmetry wave vectors, such that the stability limits are found, as determined by the local anisotropy strength relative to the dipolar coupling strength.

Keywords: magnetics, magnetic islands, frustration, dipole interactions, metastability, magnon modes.

I. REMANENT STATES IN SQUARE ARTIFICIAL SPIN ICE

Artificial spin ice on a square lattice [1] has attracted a lot of attention as a system exhibiting frustration [2, 3], a doubly-degenerate ground state [4], and monopole-like topological excitations [5–7] out of a degenerate ground state [8–10]. These properties result from the geometry-induced demagnetization anisotropy of magnetic islands fabricated on a nonmagnetic substrate [11]. Protocols using applied magnetic fields have been developed to nudge

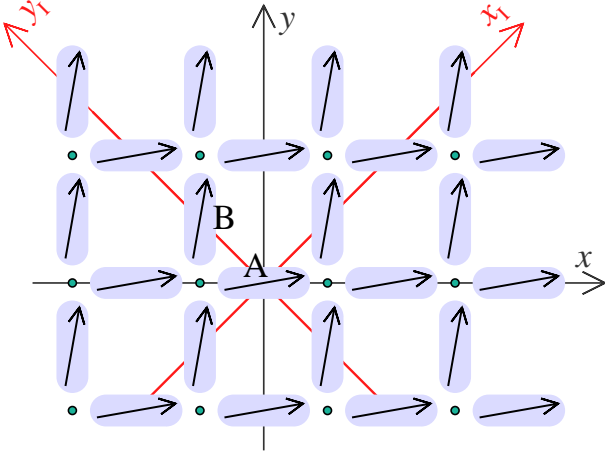


FIG. 1: Square spin ice in a remanent state magnetized along a principal NN-direction x_1 . Dots indicate the vertices, each surrounded by four islands. **A** and **B** represent the two sublattices for the two island orientations. The island lattice constant along diagonal directions is $a_I = a_v/\sqrt{2}$, where a_v is the vertex lattice constant along the original xy coordinates of the square lattice of vertices, see Eq. (2).

the system towards a ground state [12–16], which is difficult due to the energy barriers associated with frustration. In a ground state (GS) of artificial square ice, the island dipoles satisfy the two-in, two-out ice rule at each vertex to minimize the dipolar energy, also referred to as Type I, with pairs of opposing dipoles both inward or both outward across the centers of the vertices, see Fig. 1 of Ref. 17. If the system can be pushed into a ground state, it should have a particular small-amplitude spin wave spectrum, which has been investigated in varying approximations [18–20]. The spectrum is expected to help identify and characterize the ground state [21, 22].

A remanent state (RS) of spin ice, however, may be more straightforward to obtain, as it requires application of an applied field that is slowly reduced to zero. Fig. 1 shows a segment of square ice left in a remanent state, after applying a field along a nearest-neighbor (NN) primary axis of the island lattice, labeled x_1 , which was then turned off. The state is metastable, being a local energy minimum but well above the ground state, and although it also satisfies the ice rule, the vertices are of higher energy and referred to as Type II [17] vertices.

Remanent states should possess distinct small-amplitude oscillations or spinwave spectrum, that signals the presence of that state [21, 23]. The goal of the present work is to estimate the stability properties of a remanent state, by analysis of the linearized spin wave modes about a remanent state, by assuming Heisenberg-like dipole dynamics [24, 25] as opposed to Ising spins [26, 27]. There is one dipole per island, of fixed length but varying direction. This assumption ignores internal magnetization dynamics within the islands. For isolated thin islands with large in-plane aspect ratios, simulations show that there is very little spatial variation in the internal magnetization, even under a reversal process [28]. This approximation will be valid if the dipolar interaction fields are nearly uniform within an island affected by those fields.

The Heisenberg-like island dipoles in the RS of Fig. 1 are tilted slightly from the islands' long axes. This is because dipolar interactions cause the dipoles on the two

*Electronic address: wysin@phys.ksu.edu; URL: <http://www.phys.ksu.edu/personal/wysin>

sublattices to tilt towards each other as they compete with the shape anisotropy of the islands. The effects of this tilting are taken into account here.

Long-range dipole interactions have been shown to be highly relevant [29]. For clarity, we start from a NN model and extend it to include all dipolar interactions to unlimited range. The sum over infinite-range dipole interactions is motivated by a calculation of the mode spectrum for a one-dimensional chain of magnetic islands [30]. The mode spectrum helps to determine the stability properties and discriminates remanent states from other configurations.

A. Heisenberg-like dipole model

In this model [25] the magnetic islands have single-domain dipole moments of fixed magnitude μ whose time-dependent directions are along Heisenberg-like unit spin vectors $\hat{\boldsymbol{\mu}}_i(t)$. The elongation of the islands produces uniaxial anisotropy [28] along axis $\hat{\mathbf{u}}_i$ of strength K_1 , and their limited height produces planar anisotropy of strength K_3 with axis $\hat{\mathbf{z}}$. Both anisotropies are due to demagnetization or geometric effects. The anisotropy energies are very close to parabolic in the components of the dipole [28], even though small deviations from uniform magnetization can appear at the edges. The islands are elongated either along the x or y directions of a square lattice of vertices, and they are symmetrically located between vertices at locations $(v_x, v_y)a_v$, where the spacing is a_v and v_x, v_y are integer locations. The Hamiltonian for N islands can be written

$$H = -\frac{\mu_0 \mu^2}{4\pi a_1^3} \sum_{i>j}^N \frac{[3(\hat{\boldsymbol{\mu}}_i \cdot \hat{\mathbf{r}}_{ij})(\hat{\boldsymbol{\mu}}_j \cdot \hat{\mathbf{r}}_{ij}) - \hat{\boldsymbol{\mu}}_i \cdot \hat{\boldsymbol{\mu}}_j]}{(r_{ij}/a_1)^3} + \sum_i \{K_1[1 - (\hat{\boldsymbol{\mu}}_i \cdot \hat{\mathbf{u}}_i)^2] + K_3(\hat{\boldsymbol{\mu}}_i \cdot \hat{\mathbf{z}})^2\} \quad (1)$$

where μ_0 is the magnetic permeability of space, a_1 is the NN-spacing of the islands and r_{ij} and $\hat{\mathbf{r}}_{ij}$ are center-to-center distance and direction vectors between pairs of islands [31]. The NN island separation is $a_1 = \frac{1}{\sqrt{2}}a_v$, which determines the NN principal displacements (i.e., basis vectors of the island lattice),

$$\mathbf{x}_1 = \frac{1}{\sqrt{2}}a_1(\hat{\mathbf{x}} + \hat{\mathbf{y}}), \quad \mathbf{y}_1 = \frac{1}{\sqrt{2}}a_1(-\hat{\mathbf{x}} + \hat{\mathbf{y}}), \quad (2)$$

rotated 45° from the xy coordinate system of the vertices, see Fig. 1. When indicating directions in this work, the island NN principal directions along $\hat{\mathbf{x}}_1$ and $\hat{\mathbf{y}}_1$ are used. For example, the net magnetization of the state in Fig. 1 is along the [10] direction of the island lattice (equivalent to the [11] direction of the vertex lattice).

A convenient energy unit is the NN dipolar coupling, denoted with script \mathcal{D} ,

$$\mathcal{D} \equiv \frac{\mu_0 \mu^2}{4\pi a_1^3}, \quad (3)$$

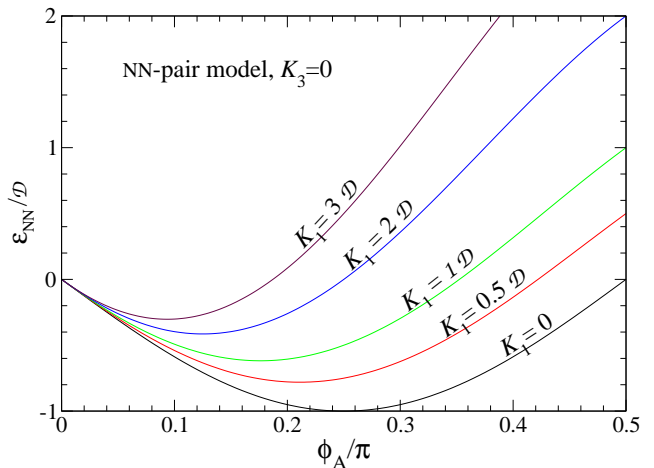


FIG. 2: The RS energy $\varepsilon_{\text{NN}}(\phi_A)$ given in Eq. (10) for various values of in-plane anisotropy, K_1/\mathcal{D} . In all cases there is a local minimum, which suggests real frequencies of oscillation about that minimum, however, the NN-model requires $K_1 > 2.947\mathcal{D}$ for stability, which limits the stable canting angle ϕ_A .

and farther neighbors have dipole interactions reduced by the center-to-center distance cubed.

II. REMANENT STATES IN THE NN-MODEL

First we consider only NN dipole interactions, and later include long-range interactions that are known to be important [32, 33] in the dynamics of spin ice. The system is assumed to be uniform by sublattice. The islands aligned along $\hat{\mathbf{x}}$ make up the A sublattice, with spins $\hat{\boldsymbol{\mu}}_i=\mathbf{A}$, and the islands aligned along $\hat{\mathbf{y}}$ comprise the B sublattice, with spins $\hat{\boldsymbol{\mu}}_i=\mathbf{B}$. A central A-site interacts with four NN B-sites, and *vice-versa*. The dipole interactions depend on the direction to the neighbors.

Taking the interaction of an A-site with its neighbors, averaged with the interaction of a B-site with its neighbors, leads to an effective two-sublattice Hamiltonian, which is the energy per pair of A and B sites,

$$H_{\text{AB}} = -2\mathcal{D} [3(\mathbf{A} \cdot \hat{\mathbf{x}}_1)(\mathbf{B} \cdot \hat{\mathbf{x}}_1) + 3(\mathbf{A} \cdot \hat{\mathbf{y}}_1)(\mathbf{B} \cdot \hat{\mathbf{y}}_1) - 2\mathbf{A} \cdot \mathbf{B}] + K_1(2 - A_x^2 - B_y^2) + K_3(A_z^2 + B_z^2). \quad (4)$$

Inserting the NN unit vectors, this is

$$H_{\text{AB}} = -2\mathcal{D}(A_x B_x + A_y B_y - 2A_z B_z) + K_1(2 - A_x^2 - B_y^2) + K_3(A_z^2 + B_z^2). \quad (5)$$

A local minimum of this Hamiltonian is a remanent state. It should be minimized under the constraint of fixed spin length for \mathbf{A} and \mathbf{B} . Lagrange's method of undetermined multipliers quickly shows that $A_z = B_z = 0$ is required; the dipoles remain within the xy -plane. Thus their equilibrium directions are described by in-plane angles ϕ_A and ϕ_B , taken as counterclockwise deviations away from

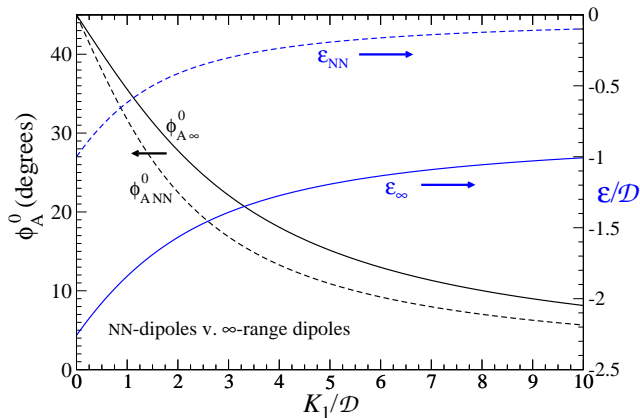


FIG. 3: The RS equilibrium tilting angles ϕ_A^0 (left axis) given in Eqs. 9, and the equilibrium energy per site ε (right axis) in Eqs. 10, as functions of the islands' uniaxial anisotropy K_1/\mathcal{D} , comparing the nearest-neighbor couplings model with the infinite-range couplings model in Sec. IV A.

the $\hat{\mathbf{x}}$ and $\hat{\mathbf{y}}$ directions, such that,

$$\mathbf{A} = (\cos \phi_A, \sin \phi_A, 0), \quad \mathbf{B} = (-\sin \phi_B, \cos \phi_B, 0). \quad (6)$$

In these coordinates the two-sublattice Hamiltonian is

$$H_{AB} = -2\mathcal{D} \sin(\phi_A - \phi_B) + K_1(2 - \cos^2 \phi_A - \cos^2 \phi_B). \quad (7)$$

This is minimized when $\sin 2\phi_A = -\sin 2\phi_B$, which implies $\phi_B = -\phi_A$, together with the additional requirement,

$$\frac{\partial H_{AB}}{\partial \phi_A} = -2\mathcal{D} \cos(\phi_A - \phi_B) + K_1 \sin 2\phi_A = 0. \quad (8)$$

The fourfold symmetry of the system implies four RS solutions. We consider the primary one as that where the system magnetization points at 45° between the x and y axes (along \mathbf{x}_I), with energy-minimizing angles satisfying

$$\tan 2\phi_A^0 = -\tan 2\phi_B^0 = \frac{2\mathcal{D}}{K_1}. \quad (9)$$

The 0 superscript indicates the equilibrium RS values. With ϕ_A^0 positive, and ϕ_B^0 negative, as in Fig. 1, the sublattices tilt inward towards the 45° diagonal direction, attempting to minimize dipolar energy which competes with an increasing uniaxial anisotropy energy. The inward canting of the sublattices is small, unless K_1 is small. However, when K_1 is too small the state will destabilize, as is shown later. Thus there is a limited amount of spin canting.

With $\phi_B = -\phi_A$, the energy per site is

$$\varepsilon_{NN}(\phi_A) = \frac{1}{2}H_{AB} = -\mathcal{D} \sin 2\phi_A + K_1 \sin^2 \phi_A. \quad (10)$$

This is minimized when $\phi_A = \phi_A^0$, as seen in Fig. 2 for various anisotropy strengths relative to dipole strength. Stronger uniaxial anisotropy in the islands reduces the spin canting, see Fig. 3, which shows the canting angle ϕ_A^0 and energy per site ε_{NN} for the NN-model and

for the model that includes infinite-range dipole interactions, below. For comparison, the per-site energy in a ground state of square ice is $\varepsilon_{gs} = -3\mathcal{D}$ when only NN-interactions are included. Later we show that the NN-model requires $K_1 > 2.947\mathcal{D}$ for RS stability, hence the NN canting angle is limited by $\phi_A^0 < 17^\circ$. Even so, this angular deviation must be taken into account to obtain correct normal mode oscillation frequencies around a remanent state.

III. LINEARIZED OSCILLATION DYNAMICS IN THE NN-MODEL

Still staying with the NN-model, the small amplitude oscillations can be analyzed. The island dipoles are now allowed to deviate slightly from their equilibrium RS directions in Eq. (9), including out-of-plane deviations $\mu_{\mathbf{n}}^z = \mu \sin \theta_{\mathbf{n}}$. An island is located at

$$\mathbf{n} = n_{x_I}\mathbf{x}_I + n_{y_I}\mathbf{y}_I, \quad (11)$$

in terms of the NN principal displacements $\mathbf{x}_I, \mathbf{y}_I$, letting $n_{x_I} = 1, 2, 3, \dots, N_1$ and $n_{y_I} = 1, 2, 3, \dots, N_2$. The total energy is a sum over islands \mathbf{n} , and counting the dipole interactions with a NN bond to $\mathbf{n} + \mathbf{x}_I$ and a NN bond to $\mathbf{n} + \mathbf{y}_I$. The dipole interaction energies in these different directions are not equivalent.

Based on (1), the dipole-dipole interaction energy of an island at \mathbf{n} on the A-sublattice with the neighbor at $\mathbf{n} + \mathbf{x}_I$ on the B-sublattice is

$$u_{\text{dd}\parallel} = -\mathcal{D} \left[\frac{3}{2}(A_{\mathbf{n}}^x B_{\mathbf{n}+\mathbf{x}_I}^y + A_{\mathbf{n}}^y B_{\mathbf{n}+\mathbf{x}_I}^x) + \frac{1}{2}(A_{\mathbf{n}}^x B_{\mathbf{n}+\mathbf{x}_I}^x + A_{\mathbf{n}}^y B_{\mathbf{n}+\mathbf{x}_I}^y) - A_{\mathbf{n}}^z B_{\mathbf{n}+\mathbf{x}_I}^z \right]. \quad (12)$$

The parallel symbol (\parallel) indicates that the spins point close to the bond direction. For the interaction of an A-site with its neighbor at $\mathbf{n} + \mathbf{y}_I$ on the B-sublattice, the first term has the opposite sign,

$$u_{\text{dd}\perp} = -\mathcal{D} \left[-\frac{3}{2}(A_{\mathbf{n}}^x B_{\mathbf{n}+\mathbf{y}_I}^y + A_{\mathbf{n}}^y B_{\mathbf{n}+\mathbf{y}_I}^x) + \frac{1}{2}(A_{\mathbf{n}}^x B_{\mathbf{n}+\mathbf{y}_I}^x + A_{\mathbf{n}}^y B_{\mathbf{n}+\mathbf{y}_I}^y) - A_{\mathbf{n}}^z B_{\mathbf{n}+\mathbf{y}_I}^z \right]. \quad (13)$$

The perpendicular symbol (\perp) indicates that the spins point almost perpendicular to the bond direction. These expressions also apply to the interaction of a B-island with its principal direction neighbors on the A-sublattice (interchanging A and B).

To analyze time-dependent fluctuations, the in-plane angles are set to $\phi_A = \phi_A^0 + \phi_{\mathbf{n}}(t)$ on A-islands and $\phi_B = \phi_B^0 + \phi_{\mathbf{n}}(t)$ on B-islands, where $\phi_{\mathbf{n}}(t)$ are the deviations from the equilibrium RS. There are nonzero out-of-plane deviations $\theta_{\mathbf{n}}(t)$, such that the spins' (x, y, z) components are written

$$\begin{aligned} \mathbf{A}_{\mathbf{n}} &= (c_{\mathbf{n}} \cos(\phi_A^0 + \phi_{\mathbf{n}}), c_{\mathbf{n}} \sin(\phi_A^0 + \phi_{\mathbf{n}}), s_{\mathbf{n}}), \\ \mathbf{B}_{\mathbf{n}} &= (-c_{\mathbf{n}} \sin(-\phi_A^0 + \phi_{\mathbf{n}}), c_{\mathbf{n}} \cos(-\phi_A^0 + \phi_{\mathbf{n}}), s_{\mathbf{n}}), \end{aligned} \quad (14)$$

where $c_{\mathbf{n}} = \cos \theta_{\mathbf{n}}$, $s_{\mathbf{n}} = \sin \theta_{\mathbf{n}}$.

Then, the dipolar energies can be expanded to quadratic order in $\phi_{\mathbf{n}} \ll 1$ and $\theta_{\mathbf{n}} \ll 1$. For example,

$$\begin{aligned} \frac{u_{\text{dd}\parallel}}{\mathcal{D}} &\approx -\frac{3}{2} \left[1 - \phi_{\mathbf{n}}\phi_{\mathbf{n}+\mathbf{x}_I} - \frac{1}{2} (\phi_{\mathbf{n}}^2 + \phi_{\mathbf{n}+\mathbf{x}_I}^2 + \theta_{\mathbf{n}}^2 + \theta_{\mathbf{n}+\mathbf{x}_I}^2) \right] + \theta_{\mathbf{n}}\theta_{\mathbf{n}+\mathbf{x}_I} \\ &\quad - \frac{1}{2} \left\{ \sin(2\phi_A^0) \left[1 + \phi_{\mathbf{n}}\phi_{\mathbf{n}+\mathbf{x}_I} - \frac{1}{2} (\phi_{\mathbf{n}}^2 + \phi_{\mathbf{n}+\mathbf{x}_I}^2 + \theta_{\mathbf{n}}^2 + \theta_{\mathbf{n}+\mathbf{x}_I}^2) \right] + \cos(2\phi_A^0)(\phi_{\mathbf{n}} - \phi_{\mathbf{n}+\mathbf{x}_I}) \right\}. \end{aligned} \quad (15)$$

A similar expression gives $u_{\text{dd}\perp}$, with the $-\frac{3}{2}$ changed to $+\frac{3}{2}$. Combining $u_{\text{dd}\parallel}$ with $u_{\text{dd}\perp}$, and summing over \mathbf{n} produces the net NN dipolar energy, ordered by zeroth, linear, and quadratic terms,

$$\begin{aligned} U_{\text{dd}} &\approx -N\mathcal{D}\sin(2\phi_A^0) - \mathcal{D}\cos(2\phi_A^0) \sum_{\mathbf{n}} \left[\phi_{\mathbf{n}} - \frac{1}{2}(\phi_{\mathbf{n}+\mathbf{x}_I} + \phi_{\mathbf{n}+\mathbf{y}_I}) \right] \\ &\quad + \mathcal{D} \sum_{\mathbf{n}} \left\{ \frac{3}{2}\phi_{\mathbf{n}}(\phi_{\mathbf{n}+\mathbf{x}_I} - \phi_{\mathbf{n}+\mathbf{y}_I}) + \theta_{\mathbf{n}}(\theta_{\mathbf{n}+\mathbf{x}_I} + \theta_{\mathbf{n}+\mathbf{y}_I}) + \sin(2\phi_A^0) [\phi_{\mathbf{n}}^2 + \theta_{\mathbf{n}}^2 - \frac{1}{2}\phi_{\mathbf{n}}(\phi_{\mathbf{n}+\mathbf{x}_I} + \phi_{\mathbf{n}+\mathbf{y}_I})] \right\}. \end{aligned} \quad (16)$$

In the same way, the anisotropy energy after expansion is

$$U_K \approx NK_1 \sin^2 \phi_A^0 + \frac{K_1}{2} \sin(2\phi_A^0) \sum_{\mathbf{n}} \left[\phi_{\mathbf{n}} - \frac{1}{2}(\phi_{\mathbf{n}+\mathbf{x}} + \phi_{\mathbf{n}+\mathbf{y}}) \right] + \sum_{\mathbf{n}} \left[K_1 \cos(2\phi_A^0) \phi_{\mathbf{n}}^2 + (K_1 \cos^2 \phi_A^0 + K_3) \theta_{\mathbf{n}}^2 \right]. \quad (17)$$

The total system energy is the sum,

$$H = U_{\text{dd}} + U_K = H^0 + H^{(1)} + H^{(2)}, \quad (18)$$

where the zeroth order term $H^{(0)}$ is the RS energy:

$$H^{(0)} = N \left(-\mathcal{D} \sin 2\phi_A^0 + K_1 \sin^2 \phi_A^0 \right). \quad (19)$$

The term $H^{(1)}$ linear in deviations is zero, and the quadratic terms are separated into in-plane parts and out-of-plane parts, $H^{(2)} = H_{\phi} + H_{\theta}$, defined by

$$\begin{aligned} H_{\phi} &= \sum_{\mathbf{n}} \left\{ [\mathcal{D} \sin 2\phi_A^0 + K_1 \cos 2\phi_A^0] \phi_{\mathbf{n}}^2 \right. \\ &\quad \left. - \frac{1}{2}\mathcal{D} \sin(2\phi_A^0) \phi_{\mathbf{n}}(\phi_{\mathbf{n}+\mathbf{x}_I} + \phi_{\mathbf{n}+\mathbf{y}_I}) \right. \\ &\quad \left. + \frac{3}{2}\mathcal{D} \phi_{\mathbf{n}}(\phi_{\mathbf{n}+\mathbf{x}_I} - \phi_{\mathbf{n}+\mathbf{y}_I}) \right\}, \end{aligned} \quad (20)$$

$$\begin{aligned} H_{\theta} &= \sum_{\mathbf{n}} \left\{ [\mathcal{D} \sin 2\phi_A^0 + K_1 \cos^2 \phi_A^0 + K_3] \theta_{\mathbf{n}}^2 \right. \\ &\quad \left. + \mathcal{D} \theta_{\mathbf{n}}(\theta_{\mathbf{n}+\mathbf{x}_I} + \theta_{\mathbf{n}+\mathbf{y}_I}) \right\}. \end{aligned} \quad (21)$$

A. Spin deviation energy in matrix form

Having expressed the small fluctuations by quadratic Hamiltonians, now it is possible to extract the modes of oscillation. To that end, the sub-Hamiltonians H_{ϕ} and H_{θ} can be written in a matrix notation, from which the spin dynamics is easier to follow. Generally, the spin deviations form state vectors (written as row vectors),

$$\begin{aligned} \psi_{\phi}^{\dagger} &= (\phi_1, \phi_2, \phi_3, \dots, \phi_N), \\ \psi_{\theta}^{\dagger} &= (\theta_1, \theta_2, \theta_3, \dots, \theta_N), \end{aligned} \quad (22)$$

where the subscripts label the islands. There are only sparse couplings (i.e., nearest neighbors) among the elements of each vector. The out-of-plane Hamiltonian can

be written in terms of an $N \times N$ matrix \mathbf{M}_{θ} as

$$H_{\theta} = \frac{1}{2} \psi_{\theta}^{\dagger} \mathbf{M}_{\theta} \psi_{\theta}, \quad (23)$$

where the matrix elements are either diagonal ones ($M_{\theta, \mathbf{n}, \mathbf{n}}$) or NN ones ($M_{\theta, \mathbf{n}, \mathbf{n} \pm \mathbf{x}_I}$ and $M_{\theta, \mathbf{n}, \mathbf{n} \pm \mathbf{y}_I}$). From (21), the nonzero elements are

$$\begin{aligned} M_{\theta, \mathbf{n}, \mathbf{n}} &= M_{\theta, 1} \equiv 2 (\mathcal{D} \sin 2\phi_A^0 + K_1 \cos^2 \phi_A^0 + K_3), \\ M_{\theta, \mathbf{n}, \mathbf{n} \pm \mathbf{x}_I} &= M_{\theta, \mathbf{n}, \mathbf{n} \pm \mathbf{y}_I} \equiv M_{\theta, 2} = \mathcal{D}. \end{aligned} \quad (24)$$

M_{θ} is symmetric: $M_{\theta, \mathbf{n}, \mathbf{m}} = M_{\theta, \mathbf{m}, \mathbf{n}}$. The in-plane Hamiltonian can be written in the same form,

$$H_{\phi} = \frac{1}{2} \psi_{\phi}^{\dagger} \mathbf{M}_{\phi} \psi_{\phi}, \quad (25)$$

where (20) gives the nonzero matrix elements,

$$\begin{aligned} M_{\phi, \mathbf{n}, \mathbf{n}} &= M_{\phi, 1} \equiv 2 (\mathcal{D} \sin 2\phi_A^0 + K_1 \cos 2\phi_A^0), \\ M_{\phi, 2} &\equiv -\frac{1}{2}\mathcal{D} \sin 2\phi_A^0, \quad M_{\phi, 3} \equiv \frac{3}{2}\mathcal{D}, \\ M_{\phi, \mathbf{n}, \mathbf{n} \pm \mathbf{x}_I} &= M_{\phi, 2} + M_{\phi, 3}, \\ M_{\phi, \mathbf{n}, \mathbf{n} \pm \mathbf{y}_I} &= M_{\phi, 2} - M_{\phi, 3}. \end{aligned} \quad (26)$$

\mathbf{M}_{ϕ} is also symmetric, but the couplings in the \mathbf{y}_I direction are different than those in the \mathbf{x}_I direction.

B. Spin dynamics from H_{ϕ} and H_{θ}

Assuming a gyromagnetic ratio γ_e , the undamped dynamics of an island's magnetic moment is given by a torque equation [34, 35],

$$\frac{d\boldsymbol{\mu}_{\mathbf{n}}}{dt} = \gamma_e \boldsymbol{\mu}_{\mathbf{n}} \times \mathbf{B}_{\mathbf{n}}. \quad (27)$$

The magnetic field that acts on an island is derived from the total Hamiltonian, $H = H_{\phi} + H_{\theta}$, according to

$$\mathbf{B}_{\mathbf{n}} = -\frac{\partial H}{\partial \boldsymbol{\mu}_{\mathbf{n}}}. \quad (28)$$

Each island's unit spin $\hat{\boldsymbol{\mu}}_{\mathbf{n}}$ is nearly aligned to the equilibrium magnetic field $\mathbf{B}_{\mathbf{n}}^0$ acting on it, except for the small deviations caused by oscillations. The fluctuations in $\mathbf{B}_{\mathbf{n}}$ contribute to torque. Let $\hat{\boldsymbol{\mu}}_{\mathbf{n}}^0$ be the equilibrium spin, and then let $\hat{\mathbf{t}}_{\mathbf{n}} = \hat{\mathbf{z}} \times \hat{\boldsymbol{\mu}}_{\mathbf{n}}^0$ be a unit vector transverse to $\hat{\boldsymbol{\mu}}_{\mathbf{n}}^0$ in the xy -plane. The spin has transverse deviation $\phi_{\mathbf{n}} \hat{\mathbf{t}}_{\mathbf{n}}$ and z -deviation $\theta_{\mathbf{n}} \hat{\mathbf{z}}$, such that

$$\hat{\boldsymbol{\mu}}_{\mathbf{n}} \approx \hat{\boldsymbol{\mu}}_{\mathbf{n}}^0 + \phi_{\mathbf{n}} \hat{\mathbf{t}}_{\mathbf{n}} + \theta_{\mathbf{n}} \hat{\mathbf{z}}. \quad (29)$$

The magnetic field can also be expressed as the equilibrium value plus transverse and z -deviations,

$$\mathbf{B}_{\mathbf{n}} = \mathbf{B}_{\mathbf{n}}^0 - \frac{1}{\mu} \frac{\partial H}{\partial \phi_{\mathbf{n}}} \hat{\mathbf{t}}_{\mathbf{n}} - \frac{1}{\mu} \frac{\partial H}{\partial \theta_{\mathbf{n}}} \hat{\mathbf{z}}. \quad (30)$$

Inserting into the torque equation (27), and keeping only leading terms, gives

$$\dot{\phi}_{\mathbf{n}} \hat{\mathbf{t}}_{\mathbf{n}} + \dot{\theta}_{\mathbf{n}} \hat{\mathbf{z}} = \gamma_e \hat{\boldsymbol{\mu}}_{\mathbf{n}}^0 \times \left(\mathbf{B}_{\mathbf{n}}^0 - \frac{1}{\mu} \frac{\partial H}{\partial \phi_{\mathbf{n}}} \hat{\mathbf{t}}_{\mathbf{n}} - \frac{1}{\mu} \frac{\partial H}{\partial \theta_{\mathbf{n}}} \hat{\mathbf{z}} \right). \quad (31)$$

Separating into transverse and z -components gives the linearized Hamiltonian equations of motion,

$$\dot{\phi}_{\mathbf{n}} = \frac{\gamma_e}{\mu} \frac{\partial H}{\partial \theta_{\mathbf{n}}}, \quad \dot{\theta}_{\mathbf{n}} = -\frac{\gamma_e}{\mu} \frac{\partial H}{\partial \phi_{\mathbf{n}}}. \quad (32)$$

These result more directly by realizing that out-of-plane component $\hat{\boldsymbol{\mu}}_{\mathbf{n}}^z = \theta_{\mathbf{n}}$ is the momentum conjugate to $\phi_{\mathbf{n}}$.

With $H = H_{\phi} + H_{\theta}$ in separated form, the set of derivatives can be expressed via matrix notation,

$$\left(\frac{\partial H_{\phi}}{\partial \phi_{\mathbf{n}}} \right) = \mathbf{M}_{\phi} \psi_{\phi}, \quad \left(\frac{\partial H_{\theta}}{\partial \theta_{\mathbf{n}}} \right) = \mathbf{M}_{\theta} \psi_{\theta}. \quad (33)$$

The dynamic equations become a matrix problem with $2N$ degrees of freedom,

$$\dot{\psi}_{\phi} = \frac{\gamma_e}{\mu} \mathbf{M}_{\theta} \psi_{\theta}, \quad \dot{\psi}_{\theta} = -\frac{\gamma_e}{\mu} \mathbf{M}_{\phi} \psi_{\phi}. \quad (34)$$

There are various ways to solve (34) for the dynamic eigenmodes. One way that works only in the NN-model is to find the eigenvalues and eigenvectors of \mathbf{M}_{θ} and \mathbf{M}_{ϕ} , that satisfy

$$\mathbf{M}_{\theta} \psi_{\theta} = \lambda_{\theta} \psi_{\theta}, \quad \mathbf{M}_{\phi} \psi_{\phi} = \lambda_{\phi} \psi_{\phi}. \quad (35)$$

1. Eigenvalues of \mathbf{M}_{θ}

Consider \mathbf{M}_{θ} . The elements $\theta_{\mathbf{n}}$ of an eigenvector are identified by their position, $\mathbf{n} = n_{x_1} \mathbf{x}_{1I} + n_{y_1} \mathbf{y}_{1I}$, in the NN island coordinates. One row of the eigenvalue problem for \mathbf{M}_{θ} is

$$M_{\theta,1} \theta_{\mathbf{n}} + M_{\theta,2} (\theta_{\mathbf{n}+\mathbf{x}_1} + \theta_{\mathbf{n}-\mathbf{x}_1}) + M_{\theta,2} (\theta_{\mathbf{n}+\mathbf{y}_1} + \theta_{\mathbf{n}-\mathbf{y}_1}) = \lambda_{\theta} \theta_{\mathbf{n}}, \quad (36)$$

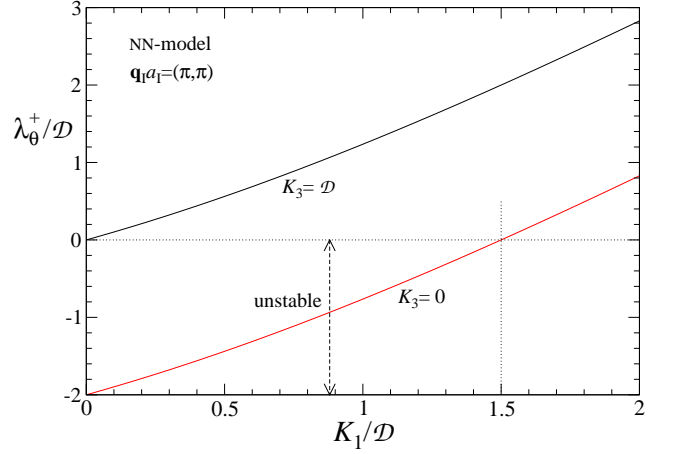


FIG. 4: Energy eigenvalue λ_{θ}^+ vs. in-plane anisotropy, for the most unstable wave vector $\mathbf{q}_{1a_1} = (\pi, \pi)$ in island coordinates, showing that stability requires $K_1 > 1.5D$ when $K_3 = 0$, or any $K_1 > 0$ when $K_3 > D$. The same results hold for $\lambda_{\theta}^-(0, 0)$.

where the on-site ($M_{\theta,1}$) and NN ($M_{\theta,2}$) matrix elements were defined in (24). The out-of-plane fluctuations for a dipole are $\mu_{\mathbf{n}}^z = \mu \sin \theta_{\mathbf{n}} \approx \mu \theta_{\mathbf{n}}$.

With periodic boundary conditions, wave solutions result. The elements of ψ_{θ} are either on the A or B sublattice. Thus two amplitudes a_{θ}, b_{θ} are included, *i.e.*,

$$\begin{aligned} \theta_{\mathbf{n}}^A &= a_{\theta} e^{i\mathbf{q} \cdot \mathbf{n}}, \text{ A-sites,} \\ \theta_{\mathbf{n}}^B &= b_{\theta} e^{i\mathbf{q} \cdot \mathbf{n}}, \text{ B-sites.} \end{aligned} \quad (37)$$

The wave vectors $\mathbf{q} = (q_{x_1}, q_{y_1})$ are quantized in the usual way, with components in island coordinates,

$$\begin{aligned} q_{x_1} &= \frac{2\pi k_x}{N_1 a_1}, \quad k_x = 0, 1, 2, \dots (N_1 - 1), \\ q_{y_1} &= \frac{2\pi k_y}{N_2 a_1}, \quad k_y = 0, 1, 2, \dots (N_2 - 1). \end{aligned} \quad (38)$$

For the wave solution, the sums over NN's are

$$\begin{aligned} \theta_{\mathbf{n}+\mathbf{x}_1} + \theta_{\mathbf{n}-\mathbf{x}_1} &= 2\theta_{\mathbf{n}} \cos q_{x_1} a_1, \\ \theta_{\mathbf{n}+\mathbf{y}_1} + \theta_{\mathbf{n}-\mathbf{y}_1} &= 2\theta_{\mathbf{n}} \cos q_{y_1} a_1. \end{aligned} \quad (39)$$

The total \mathbf{q} -dependent phase factor is

$$\gamma_{\mathbf{q}}^+ = 2(\cos q_{x_1} a_1 + \cos q_{y_1} a_1) \quad (40)$$

The system of equations (36) is split into two sets, depending on whether \mathbf{n} resides on the A or B sublattice, producing a 2×2 reduced system:

$$\begin{bmatrix} M_{\theta,1} & M_{\theta,2} \gamma_{\mathbf{q}}^+ \\ M_{\theta,2} \gamma_{\mathbf{q}}^+ & M_{\theta,1} \end{bmatrix} \begin{bmatrix} a_{\theta} \\ b_{\theta} \end{bmatrix} = \lambda_{\theta} \begin{bmatrix} a_{\theta} \\ b_{\theta} \end{bmatrix}. \quad (41)$$

This matrix has symmetric and antisymmetric eigenvectors, $(a_{\theta}, b_{\theta}) = (\psi^{\pm})^{\dagger} \equiv \frac{1}{\sqrt{2}}(1, \pm 1)$, with eigenvalues

$$\lambda_{\theta}^{\pm} = M_{\theta,1} \pm M_{\theta,2} \gamma_{\mathbf{q}}^+. \quad (42)$$

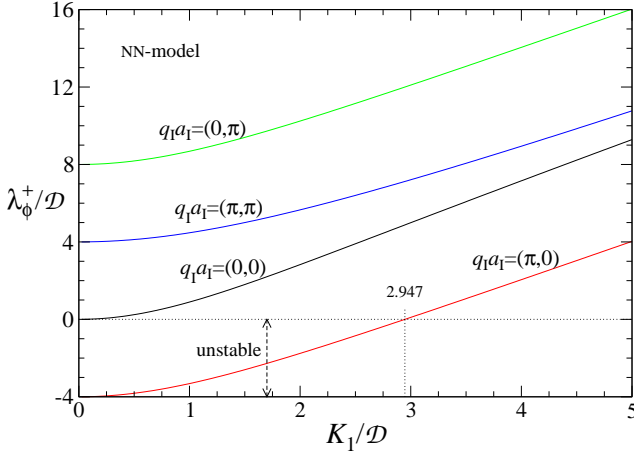


FIG. 5: The NN-model in-plane energy eigenvalue λ_ϕ^+ vs. in-plane anisotropy, for various wave vectors in island coordinates, Eq. 49, showing that stability requires $K_1 > K_{1,\min} \approx 2.947 \mathcal{D}$.

In terms of the original constants in H and with full \mathbf{q} -dependence this is

$$\lambda_\theta^\pm(\mathbf{q}) = 2 [\mathcal{D} \sin 2\phi_A^0 + K_1 \cos^2 \phi_A^0 + K_3 \pm \mathcal{D} (\cos q_{x_1} a_I + \cos q_{y_1} a_I)]. \quad (43)$$

A negative eigenvalue implies that the RS can lower its energy by excitation with the associated wave vector, which indicates instability. Specifically of interest, $\lambda_\theta^+(\pi, \pi)$ is plotted in Fig. 4, which shows RS instability for $K_1 > 1.5\mathcal{D}$ when $K_3 = 0$, and stability for all $K_1 > 0$ when $K_3 > \mathcal{D}$. Note that wave vectors are denoted in terms of their components and directions in the island coordinates.

2. Eigenvalues of \mathbf{M}_ϕ

Next, consider \mathbf{M}_ϕ , which has the matrix elements in (26). Fluctuations in $\phi_{\mathbf{n}}$ are dipole components *transverse* to the equilibrium directions, within the xy -plane. One row of the eigenvalue problem is

$$M_{\phi,1} \phi_{\mathbf{n}} + (M_{\phi,2} + M_{\phi,3})(\phi_{\mathbf{n}+\mathbf{x}_I} + \phi_{\mathbf{n}-\mathbf{x}_I}) + (M_{\phi,2} - M_{\phi,3})(\phi_{\mathbf{n}+\mathbf{y}_I} + \phi_{\mathbf{n}-\mathbf{y}_I}) = \lambda_\phi \phi_{\mathbf{n}}. \quad (44)$$

Note that couplings along the \mathbf{y}_I direction are different than along \mathbf{x}_I . Again a wave solution is present, with amplitudes a_ϕ, b_ϕ on the sublattices, *i.e.*,

$$\begin{aligned} \phi_{\mathbf{n}}^A &= a_\phi e^{i\mathbf{q}\cdot\mathbf{n}}, \text{ A-sites,} \\ \phi_{\mathbf{n}}^B &= b_\phi e^{i\mathbf{q}\cdot\mathbf{n}}, \text{ B-sites.} \end{aligned} \quad (45)$$

Defining another phase factor,

$$\gamma_{\mathbf{q}}^- = 2(\cos q_{x_1} a_I - \cos q_{y_1} a_I), \quad (46)$$

the reduced 2×2 system is

$$\begin{aligned} \begin{bmatrix} n_{aa} & n_{ab} \\ n_{ba} & n_{bb} \end{bmatrix} \begin{bmatrix} a_\phi \\ b_\phi \end{bmatrix} &= \lambda_\phi \begin{bmatrix} a_\phi \\ b_\phi \end{bmatrix}. \\ n_{aa} &= n_{bb} \equiv M_{\phi,1}, \\ n_{ab} &= n_{ba} \equiv M_{\phi,2} \gamma_{\mathbf{q}}^+ + M_{\phi,3} \gamma_{\mathbf{q}}^-. \end{aligned} \quad (47)$$

The eigenvectors are again symmetric and antisymmetric, $(a_\phi, b_\phi) = (\psi^\pm)^\dagger = \frac{1}{\sqrt{2}}(1, \pm 1)$ with eigenvalues

$$\lambda_\phi^\pm = M_{\phi,1} \pm (M_{\phi,2} \gamma_{\mathbf{q}}^+ + M_{\phi,3} \gamma_{\mathbf{q}}^-). \quad (48)$$

The full dependence on \mathbf{q} and parameters in H is

$$\begin{aligned} \lambda_\phi^\pm(\mathbf{q}) &= 2K_1 \cos 2\phi_A^0 \pm 3\mathcal{D}(\cos q_{x_1} a_I - \cos q_{y_1} a_I) \\ &+ \mathcal{D} \sin 2\phi_A^0 [2 \mp (\cos q_{x_1} a_I + \cos q_{y_1} a_I)]. \end{aligned} \quad (49)$$

This eigenvalue has considerable dependence on wave vector, see Fig. 5. For example, λ_ϕ^+ becomes the most negative for $\mathbf{q}_I a_I = (\pi, 0)$, and additionally, it will not become positive unless $K_1 > 2.947\mathcal{D}$, approximately. This shows that a traveling mode along the x_I axis destabilizes the RS, and $K_1 > K_{1,\min} \approx 2.947 \mathcal{D}$ is required for stability in the NN-model. There is another instability where λ_ϕ^- is less than zero for $\mathbf{q}_I a_I = (0, \pi)$ when K_1 becomes less than $2.947\mathcal{D}$. Then, the stability requirement for $\lambda_\theta^+ > 0$ in Fig. 4 is satisfied even for $K_3 = 0$.

3. NN-model mode eigenfrequencies

For the NN-model only, the matrices \mathbf{M}_θ and \mathbf{M}_ϕ have the *same* eigenvectors, $(\psi^\pm)^\dagger = \frac{1}{\sqrt{2}}(1, \pm 1)$. A time derivative of equations (34) separates ϕ and θ solutions,

$$\ddot{\psi}_\phi = - \left(\frac{\gamma_e}{\mu} \right)^2 \mathbf{M}_\theta \mathbf{M}_\phi \psi_\phi, \quad (50)$$

and similarly for $\ddot{\psi}_\theta$. Either eigenvector $\psi_\phi = \psi^+$ or $\psi_\phi = \psi^-$ is a separate solution to these equations. Assuming $e^{-i\omega t}$ time dependencies, the eigenfrequencies in the NN-model only, for both θ and ϕ oscillations, which remain intrinsically coupled, are given by

$$\omega_{\text{NN}}^\pm(\mathbf{q}) = \frac{\gamma_e}{\mu} \sqrt{\lambda_\theta^\pm(\mathbf{q}) \lambda_\phi^\pm(\mathbf{q})}, \quad (51)$$

where the natural choice for frequency unit is

$$\delta_1 \equiv \frac{\gamma_e}{\mu} \mathcal{D}. \quad (52)$$

Some typical mode frequencies are shown in Fig. 6, first for anisotropy at the stability limit, $K_1 = K_{1,\min} \approx 2.947 \mathcal{D}$, with $K_3 = 0$. The wave vectors are given in the island coordinate system. The RS mode frequencies in the [10] and [01] directions are different because the net nonzero magnetization is along the [10] direction, breaking the symmetry. The most important feature is the

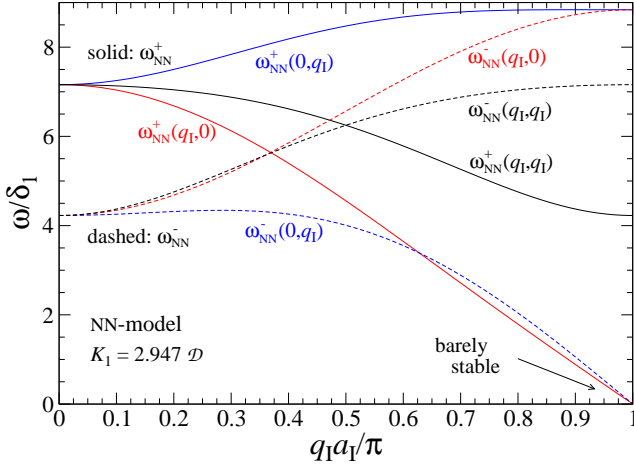


FIG. 6: The mode frequencies ω_{NN}^{\pm} in units of $\delta_1 = \gamma_e \mathcal{D} / \mu$, in the NN-model, for the minimum value, $K_1 = K_{1,\text{min}} \approx 2.947 \mathcal{D}$, that insures RS stability, together with $K_3 = 0$, for wave vectors along directions in the island principal coordinates.

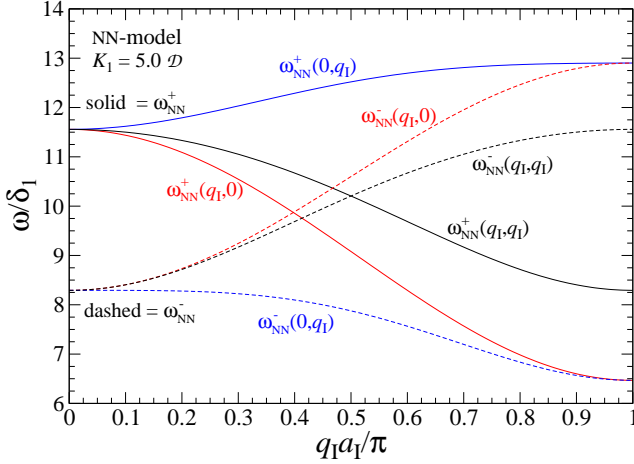


FIG. 7: The mode frequencies ω_{NN}^{\pm} in units of $\delta_1 = \gamma_e \mathcal{D} / \mu$, in the NN-model, for anisotropy $K_1 = 5.0 \mathcal{D}$, well above that needed for RS stability, together with $K_3 = 0$, for wave vectors given in the island principal coordinates.

softening of the modes in [10] and [01] directions towards zero frequency as $q_1 a_1 \rightarrow \pi$, signifying the RS instability. When the anisotropy is increased to $K_1 = 5.0 \mathcal{D}$, Fig. 7, all modes oscillate well above zero frequency.

While the frequency spectrum might be useful for experimental detection of a state, it is important to go beyond the NN-model and include the modifications due to longer range dipole interactions.

IV. EFFECTS OF LONG-RANGE-DIPOLE (LRD) INTERACTIONS

To get a better description, dipole interactions beyond NN must be included. Consider two islands' dipoles,

one at a site \mathbf{n} and another at displacement \mathbf{r} , on site $\mathbf{m} = \mathbf{n} + \mathbf{r}$. While the spins are written using their (x, y, z) components, it is best to describe the displacements in integer NN island coordinates, (x_1, y_1) , *i.e.*

$$\mathbf{r} = (x_1 \hat{\mathbf{x}}_1 + y_1 \hat{\mathbf{y}}_1) a_1, \quad (53)$$

in contrast to vertex coordinates (x, y) , meaning

$$\mathbf{r} = (x \hat{\mathbf{x}} + y \hat{\mathbf{y}}) a_v. \quad (54)$$

The transformation between the two is

$$x = \frac{1}{2}(x_1 - y_1), \quad y = \frac{1}{2}(x_1 + y_1). \quad (55)$$

When $(x_1 + y_1)$ is even (or x and y both integers), the displacement stays on the same sublattice (AA or BB bond). When $(x_1 + y_1)$ is odd (or x and y both half-integers), the displacement goes from one sublattice to the other (AB bond). The separation is $r = \sqrt{x_1^2 + y_1^2} a_1$. The dipole interaction is reduced from its NN-strength \mathcal{D} by a factor

$$\rho^3 \equiv r^3 / a_1^3 = (x_1^2 + y_1^2)^{3/2}. \quad (56)$$

From (1), the island pair dipole interaction is

$$u_{\mathbf{n}\mathbf{m}} = -\frac{\mathcal{D}}{\rho^3} \left[\left(\frac{1}{2} - \frac{3x_1 y_1}{\rho^2} \right) \mu_{\mathbf{n}}^x \mu_{\mathbf{m}}^x + \left(\frac{1}{2} + \frac{3x_1 y_1}{\rho^2} \right) \mu_{\mathbf{n}}^y \mu_{\mathbf{m}}^y + \frac{3}{2\rho^2} (x_1^2 - y_1^2) (\mu_{\mathbf{n}}^x \mu_{\mathbf{m}}^y + \mu_{\mathbf{n}}^y \mu_{\mathbf{m}}^x) - \mu_{\mathbf{n}}^z \mu_{\mathbf{m}}^z \right]. \quad (57)$$

Consider first an AB bond, where $(x_1 + y_1)$ is odd. The dipoles are labeled $\hat{\boldsymbol{\mu}}_{\mathbf{n}} = \mathbf{A}_{\mathbf{n}}$ and $\hat{\boldsymbol{\mu}}_{\mathbf{m}} = \mathbf{B}_{\mathbf{m}}$. The dipoles have slight angular deviations from the equilibrium RS, as in (14). The terms needed are expanded up to quadratic order in the deviations, such as

$$A_{\mathbf{n}}^x B_{\mathbf{m}}^x \approx c_{\mathbf{n}} c_{\mathbf{m}} \left[\left(1 - \frac{1}{2} \phi_{\mathbf{n}}^2 - \frac{1}{2} \phi_{\mathbf{m}}^2 + \phi_{\mathbf{n}} \phi_{\mathbf{m}} \right) \cos \phi_A^0 \sin \phi_A^0 - \phi_{\mathbf{n}} \sin^2 \phi_A^0 - \phi_{\mathbf{m}} \cos^2 \phi_A^0 \right], \quad (58)$$

where the out-of-plane deviation factor is

$$c_{\mathbf{n}} c_{\mathbf{m}} \approx 1 - \frac{1}{2} \theta_{\mathbf{n}}^2 - \frac{1}{2} \theta_{\mathbf{m}}^2. \quad (59)$$

There is a similar term for y components,

$$A_{\mathbf{n}}^y B_{\mathbf{m}}^y \approx c_{\mathbf{n}} c_{\mathbf{m}} \left[\left(1 - \frac{1}{2} \phi_{\mathbf{n}}^2 - \frac{1}{2} \phi_{\mathbf{m}}^2 + \phi_{\mathbf{n}} \phi_{\mathbf{m}} \right) \cos \phi_A^0 \sin \phi_A^0 + \phi_{\mathbf{n}} \cos^2 \phi_A^0 + \phi_{\mathbf{m}} \sin^2 \phi_A^0 \right]. \quad (60)$$

Finally, there is the cross coupling of components,

$$A_{\mathbf{n}}^x B_{\mathbf{m}}^y + A_{\mathbf{n}}^y B_{\mathbf{m}}^x \approx c_{\mathbf{n}} c_{\mathbf{m}} \left(1 - \frac{1}{2} \phi_{\mathbf{n}}^2 - \frac{1}{2} \phi_{\mathbf{m}}^2 - \phi_{\mathbf{n}} \phi_{\mathbf{m}} \right). \quad (61)$$

One can see that the pair's dipolar energy u_{AB} contains zeroth order, first order, and quadratic order terms.

Consider instead an AA pair with energy u_{AA} , or similarly, a BB pair, where $(x_1 + y_1)$ is even. For u_{AA} the needed expressions are

$$A_{\mathbf{n}}^x A_{\mathbf{m}}^x \approx c_{\mathbf{n}} c_{\mathbf{m}} \left[\left(1 - \frac{1}{2} \phi_{\mathbf{n}}^2 - \frac{1}{2} \phi_{\mathbf{m}}^2 \right) \cos^2 \phi_A^0 + \phi_{\mathbf{n}} \phi_{\mathbf{m}} \sin^2 \phi_A^0 - (\phi_{\mathbf{n}} + \phi_{\mathbf{m}}) \sin \phi_A^0 \cos \phi_A^0 \right], \quad (62)$$

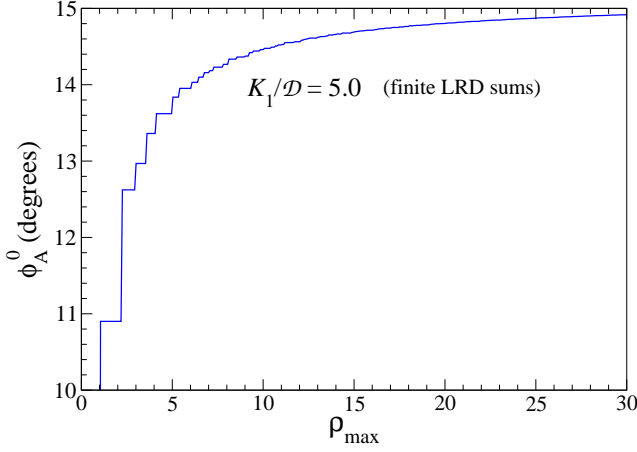


FIG. 8: The effect of adding longer-range dipole interactions on the remanent state's equilibrium tilting angle ϕ_A^0 , Eq. (72), as a function of the largest radius used in the needed sum s_{AB} of equation (70). The first large jump at $\rho_{\max} = \sqrt{5}$ is due to fourth nearest neighbors.

$$A_n^y A_m^y \approx c_n c_m \left[\left(1 - \frac{1}{2}\phi_n^2 - \frac{1}{2}\phi_m^2\right) \sin^2 \phi_A^0 + \phi_n \phi_m \cos^2 \phi_A^0 + (\phi_n + \phi_m) \sin \phi_A^0 \cos \phi_A^0 \right], \quad (63)$$

$$A_n^x A_m^y + A_n^y A_m^x \approx c_n c_m \left[\left(1 - \frac{1}{2}\phi_n^2 - \frac{1}{2}\phi_m^2 - \phi_n \phi_m\right) \sin 2\phi_A^0 + (\phi_n + \phi_m) \cos 2\phi_A^0 \right]. \quad (64)$$

For u_{BB} because the equilibrium directions are different on the B-sublattice, the expressions are also different, swapping the factors of $\sin \phi_A^0$ and $\cos \phi_A^0$,

$$B_n^x B_m^x \approx c_n c_m \left[\left(1 - \frac{1}{2}\phi_n^2 - \frac{1}{2}\phi_m^2\right) \sin^2 \phi_A^0 + \phi_n \phi_m \cos^2 \phi_A^0 - (\phi_n + \phi_m) \sin \phi_A^0 \cos \phi_A^0 \right], \quad (65)$$

$$B_n^y B_m^y \approx c_n c_m \left[\left(1 - \frac{1}{2}\phi_n^2 - \frac{1}{2}\phi_m^2\right) \cos^2 \phi_A^0 + \phi_n \phi_m \sin^2 \phi_A^0 + (\phi_n + \phi_m) \sin \phi_A^0 \cos \phi_A^0 \right], \quad (66)$$

$$B_n^x B_m^y + B_n^y B_m^x \approx c_n c_m \left[\left(1 - \frac{1}{2}\phi_n^2 - \frac{1}{2}\phi_m^2 - \phi_n \phi_m\right) \sin 2\phi_A^0 - (\phi_n + \phi_m) \cos 2\phi_A^0 \right]. \quad (67)$$

A. The shifted equilibrium

Including LRD interactions, the Hamiltonian can be expressed

$$H = H^{(0)} + H^{(1)} + H^{(2)}, \quad (68)$$

where the superscripts indicates the zeroth, linear, and quadratic terms in the deviations around equilibrium. The equilibrium still has opposing in-plane tilting, $\phi_B^0 =$

$-\phi_A^0$. The terms in H come partly from AB bonds and partly from AA bonds (nearly equivalent to BB bonds), as well as the anisotropy. At the equilibrium, the linear part $H^{(1)}$ vanishes. There are no linear terms in θ_n in H , implying that the equilibrium still has values $\theta_n = 0$ for all sites, and thus all $s_n = 0$, $c_n = 1$. The zeroth order terms, not containing θ_n nor ϕ_n , are very simple in Eqs. (57) through (67) and are easy to apply to obtain $H^{(0)}$, employing inversion symmetry of the system, and dividing by two to avoid double counting. The equilibrium energy of an island interacting with the entire system via LRD interactions, per island, $\varepsilon_\infty = H^{(0)}/N$, is found to be

$$\varepsilon_\infty = K_1 \sin^2 \phi_A^0 - \frac{\mathcal{D}}{4} \left(\sum_{x_1, y_1}^{\text{AB}} \frac{\sin 2\phi_A^0}{\rho^3} + \sum_{x_1, y_1}^{\text{AA}} \frac{1}{\rho^3} \right). \quad (69)$$

The first sum is over AB bonds, where $\rho^2 = 1, 5, 9, 13$, etc. The second sum is over AA bonds, with $\rho^2 = 2, 4, 8$, etc. Estimates of the sums are

$$s_{AB} = \sum_{x_1, y_1}^{\text{AB}} \frac{1}{\rho^3} \approx 5.8397, \quad s_{AA} = \sum_{x_1, y_1}^{\text{AA}} \frac{1}{\rho^3} \approx 3.1926. \quad (70)$$

Then with infinite-range dipole interactions, the energy per island is

$$\varepsilon_\infty = K_1 \sin^2 \phi_A^0 - \frac{1}{4} \mathcal{D} (s_{AB} \sin 2\phi_A^0 + s_{AA}). \quad (71)$$

The equilibrium tilting of the dipoles takes place at the minimum of $H^{(0)}$, which gives

$$\tan 2\phi_A^0 = -\tan 2\phi_B^0 = \frac{s_{AB} \mathcal{D}}{2K_1} \approx \frac{2.9198 \mathcal{D}}{K_1}. \quad (72)$$

Thus, the effect of infinite-range dipolar interactions is to *increase* the inward tilting of the two sublattices towards each other, compared to the NN-model [Eq. (9)], see Fig. 3. The change in tilting as longer-range dipolar interactions are included is shown Fig. 8, as a function of the maximum neighbor distance ρ_{\max} used in the sum s_{AB} , for $K_1/\mathcal{D} = 5$. The largest jump (beyond NN interactions) occurs at $\rho_{\max} = \sqrt{5}$, where ϕ_A^0 changes from 10.9° to 12.6° . This is attributed to *fourth* nearest neighbor interactions (eight AB bonds with $\rho^2 = 5$) that try to align the A and B lattices. The AA bonds do not shift the equilibrium, as the sum s_{AA} plays no role in the formula for ϕ_A^0 , but they contribute to the energy.

B. Dynamics with long-range-dipole interactions

The last term in the Hamiltonian, $H^{(2)} = H_\phi + H_\theta$, is quadratic in the small deviations ϕ_n and θ_n , and controls the dynamics, as in Eqs. (32) and (34). Equations (57) through (67) give the contributions of arbitrary range dipole interactions to $H^{(2)}$, and implicitly define the matrices \mathbf{M}_ϕ and \mathbf{M}_θ . Once LRD interactions are included,

the matrices \mathbf{M}_ϕ and \mathbf{M}_θ do not have the same eigenvectors, so a more general procedure is needed to get the dynamic modes.

The dynamics in (34) is still solved using traveling waves written in the NN island coordinates. While locating an island by $\mathbf{n} = n_{x_I}\mathbf{x}_I + n_{y_I}\mathbf{y}_I$, a displacement to another island of a dipole pair is expressed as $\mathbf{r} = x_I\mathbf{x}_I + y_I\mathbf{y}_I$. Assume waves on both sublattices varying in time as $e^{-i\omega t}$ (suppressed in the formulas), the same as in the NN-model,

$$\begin{aligned} \phi_{\mathbf{n}}^A &= a_\theta e^{i\mathbf{q}\cdot\mathbf{n}}, & \phi_{\mathbf{n}}^B &= a_\phi e^{i\mathbf{q}\cdot\mathbf{n}}, & \text{A-sites,} \\ \theta_{\mathbf{n}}^A &= b_\theta e^{i\mathbf{q}\cdot\mathbf{n}}, & \theta_{\mathbf{n}}^B &= b_\phi e^{i\mathbf{q}\cdot\mathbf{n}}, & \text{B-sites.} \end{aligned} \quad (73)$$

The allowed wave vectors were given in (38).

The matrix form of the dynamic equations (34) involves sums over matrix elements with the spin field components,

$$\begin{aligned} -i\omega\phi_{\mathbf{n}} &= \frac{\gamma_e}{\mu}(M_{\theta,\mathbf{n},\mathbf{n}}\theta_{\mathbf{n}} + \sum_{\mathbf{r}\neq 0} M_{\theta,\mathbf{n},\mathbf{n}+\mathbf{r}}\theta_{\mathbf{n}+\mathbf{r}}), \\ i\omega\theta_{\mathbf{n}} &= \frac{\gamma_e}{\mu}(M_{\phi,\mathbf{n},\mathbf{n}}\phi_{\mathbf{n}} + \sum_{\mathbf{r}\neq 0} M_{\phi,\mathbf{n},\mathbf{n}+\mathbf{r}}\phi_{\mathbf{n}+\mathbf{r}}). \end{aligned} \quad (74)$$

This pair of equations becomes four equations when both A and B sublattices are considered. The matrix elements are either within a sublattice ($M_{\mathbf{n},\mathbf{m}}^{AA}, M_{\mathbf{n},\mathbf{m}}^{BB}$) or between sublattices ($M_{\mathbf{n},\mathbf{m}}^{AB}, M_{\mathbf{n},\mathbf{m}}^{BA}$). They are derived from the quadratic terms in Eqs. (57) through (67). For example, the coefficient of $\phi_{\mathbf{n}}^2$ in $A_{\mathbf{n}}^x B_{\mathbf{m}}^x$ in (58) contributes to $M_{\phi,\mathbf{n},\mathbf{n}}^{AB}$, while the coefficient of $\phi_{\mathbf{n}}\phi_{\mathbf{m}}$ contributes to $M_{\phi,\mathbf{n},\mathbf{m}}^{AB}$.

With the wave assumption, the equations comprise coupled systems with 2×2 matrices named \mathbf{m} and \mathbf{n} for compact notation,

$$-i\omega \begin{bmatrix} a_\phi \\ b_\phi \end{bmatrix} = \begin{bmatrix} m_{aa} & m_{ab} \\ m_{ba} & m_{bb} \end{bmatrix} \begin{bmatrix} a_\theta \\ b_\theta \end{bmatrix}, \quad (75)$$

$$-i\omega \begin{bmatrix} a_\theta \\ b_\theta \end{bmatrix} = - \begin{bmatrix} n_{aa} & n_{ab} \\ n_{ba} & n_{bb} \end{bmatrix} \begin{bmatrix} a_\phi \\ b_\phi \end{bmatrix}. \quad (76)$$

This is identical to a single 4×4 eigenvalue problem,

$$\begin{bmatrix} 0 & 0 & \mathbf{m} \\ 0 & 0 & \mathbf{n} \\ \mathbf{n} & 0 & 0 \\ 0 & 0 & 0 \end{bmatrix} \begin{bmatrix} a_\phi \\ b_\phi \\ ia_\theta \\ ib_\theta \end{bmatrix} = \omega \begin{bmatrix} a_\phi \\ b_\phi \\ ia_\theta \\ ib_\theta \end{bmatrix}. \quad (77)$$

Symbolically, the 2×2 matrices off the diagonal are

$$\mathbf{m} = \frac{\gamma_e}{\mu}\mathbf{M}_\theta, \quad \mathbf{n} = \frac{\gamma_e}{\mu}\mathbf{M}_\phi, \quad (78)$$

as projected onto the traveling wave solutions. More specifically, the matrix elements of \mathbf{m} and \mathbf{n} are given by sums of the interactions as derived from $H^{(2)}$. For instance, m_{aa} comes from the AA dipole interactions as

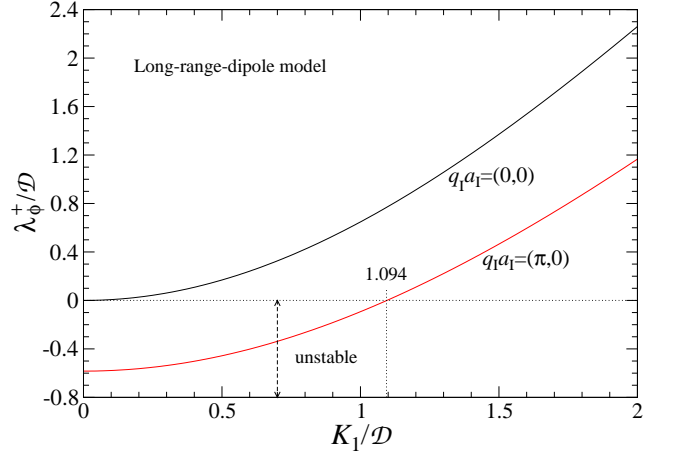


FIG. 9: With infinite-range dipole interactions, the in-plane energy eigenvalue λ_ϕ^+ vs. in-plane anisotropy, for two wave vectors in island coordinates, showing that stability requires $K_1 \gtrsim 1.094 \mathcal{D}$, significantly less than $K_1 > 2.947 \mathcal{D}$ in the NN-model.

well as the on-site anisotropy. Supposing \mathbf{n} is an A-site, with $\mathbf{n}+\mathbf{r}$ also an A-site,

$$m_{aa} = \frac{\gamma_e}{\mu} \left(M_{\theta,\mathbf{n},\mathbf{n}} + \sum_{\mathbf{r}}^{AA} M_{\theta,\mathbf{n},\mathbf{n}+\mathbf{r}} e^{i\mathbf{q}\cdot\mathbf{r}} \right). \quad (79)$$

The symbol $\sum_{\mathbf{r}}^{AA}$ indicates summing over displacements on one sublattice ($x_I + y_I = \text{even}$). The same expression gives $m_{bb} = m_{aa}$. For the AB couplings there is also symmetry,

$$m_{ab} = m_{ba} = \frac{\gamma_e}{\mu} \sum_{\mathbf{r}}^{AB} M_{\theta,\mathbf{n},\mathbf{n}+\mathbf{r}} e^{i\mathbf{q}\cdot\mathbf{r}} \quad (80)$$

where $\sum_{\mathbf{r}}^{AB}$ indicates summing over displacements from one sublattice to the other ($x_I + y_I = \text{odd}$). The full \mathbf{q} -dependence of the matrix elements of \mathbf{m} and \mathbf{n} is shown in Appendix B 1.

1. Stability requirements with LRD interactions

Similar to the NN-model, the eigenvalues of matrices \mathbf{n} and \mathbf{m} must be positive for stability of the RS when LRD interactions are included. The controlling requirement is due to the eigenvalues λ_ϕ^\pm of matrix \mathbf{n} . A general formula for its eigenvalues (as for any 2×2 matrix) is

$$\lambda_\phi^\pm = \frac{1}{2}(n_{aa} + n_{bb}) \pm \sqrt{\frac{1}{4}(n_{aa} + n_{bb})^2 - (n_{aa}n_{bb} - n_{ab}n_{ba})}. \quad (81)$$

The most unstable eigenvalue occurs at $\mathbf{q}_I = (\pi, 0)$, where the sums needed (see Appendix B 1) become

$$f_{\text{odd}}(\pi, 0) = d_{\text{evn}}(\pi, 0) = f_{\text{evn}}^{xy}(\pi, 0) = 0, \quad (82)$$

$$f_{\text{evn}}(\pi, 0) \approx -0.93546, \quad d_{\text{odd}}(\pi, 0) \approx -3.71107 \quad (83)$$

Then the eigenvalues are $\lambda_\phi^\pm = n_{aa} \pm n_{ab}$, or

$$\lambda_\phi^\pm(\pi, 0) = 2K_1 \cos 2\phi_A^0 + \frac{1}{2}\mathcal{D} [s_{AB} \sin 2\phi_A^0 + s_{AA} - f_{\text{evn}}(\pi, 0) \pm 3d_{\text{odd}}(\pi, 0)]. \quad (84)$$

Because $d_{\text{odd}}(\pi, 0)$ is negative, the eigenvalue $\lambda_\phi^+(\pi, 0)$ is smallest. It is responsible for an instability at $K_1 < 1.094 \mathcal{D}$, see Fig. 9. As a result, LRD interactions enhance the stability of the remanent state, meaning that even rather weak uniaxial anisotropy of the islands will be able to maintain that state.

2. Mode frequencies with LRD interactions

It is shown in Appendix C that the eigenfrequencies of the 4×4 eigenvalue problem (77) are obtained from

$$\omega^2 = \frac{1}{2} \left[(\mathbf{m}^T \cdot \mathbf{n}) \pm \sqrt{(\mathbf{m}^T \cdot \mathbf{n})^2 - 4|\mathbf{m}||\mathbf{n}|} \right]. \quad (85)$$

The two solutions can be labeled as $\omega_\infty^\pm(\mathbf{q})$, where ∞ indicates keeping LRD interactions to unlimited distances. The formula contains a dot product of the two 2×2 dynamic matrices, as well as a product of their determinants. It should apply to any spin dynamics problem involving a two-sublattice partitioning of the system. The two modes might be considered as acoustic and optic modes, however, such identification really depends on the spin components being considered.

Following the procedure in Appendix C, and applying Eq. 85, the dispersion relations for modes of excitation from a remanent state were obtained for various cases of anisotropy.

3. Changes in dynamics – second nearest neighbors

To see the general trend due to going beyond NN-interactions, first we include only the interactions up to second nearest neighbors (2NN), with displacements $(x, y) = (\pm 1, 0)a_v, (0, \pm 1)a_v$, which are the nearest AA or BB bonds. It is straightforward to show that the equilibrium angles ϕ_A^0 are the same as in the NN-model. The procedure in Eq. 85 gives the eigenfrequencies, using sums truncated at 2nd-nearest neighbors. A partial mode spectrum is shown in Fig. 10, for $K_1 = 2.947\mathcal{D}$, where the 2NN-model is compared to the model using infinite-range dipole interactions. The 2NN interactions already lift eigenfrequencies enough to relieve the instability that is present in the NN-model, compare Fig. 6. Once LRD-interactions to infinite range are included, the frequencies are raised further, and the notable crossing point between higher and lower modes shifts to lower frequency. Surprisingly, it is not an avoided crossing.

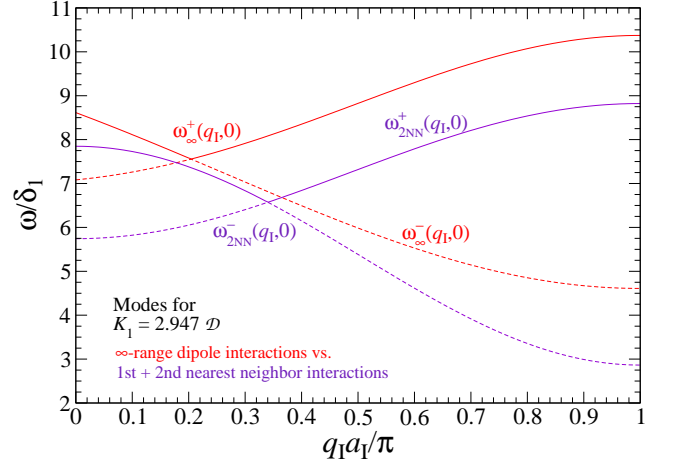


FIG. 10: Comparison of the [10] RS dispersion relations (wave vectors in island coordinates) using the 1st+2nd neighbors model ($\omega_{2\text{NN}}^\pm$, indigo) and the model with all ∞ -range dipole interactions (ω_∞^\pm , red) calculated using sums out to $\rho \approx 4000$, at $K_1 = 2.974 \mathcal{D}$, just above the minimum needed for stability in the NN-model. The frequencies are higher with more dipole terms and the crossing point shifts to lower wave vector.

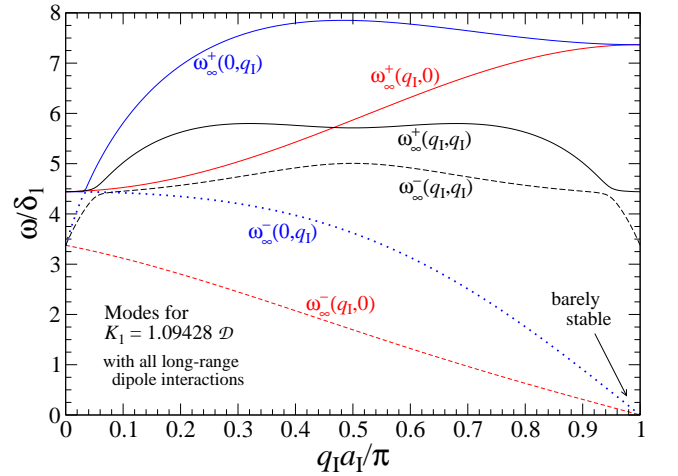


FIG. 11: Dispersion relations in island coordinates using all dipole interactions, for a remanent state with $K_1 = 1.09428 \mathcal{D}$ and $K_3 = 0$, just above the minimum needed for stability, calculated using sums out to $\rho \approx 10000$. Both the [10] and [01] ω_∞^- dispersion relations go unstable at $q_1 a_1 = \pi$ for smaller K_1 .

4. Changes in dynamics – infinite range dipole interactions

The stability limit at $K_1 \approx 1.094 \mathcal{D}, K_3 = 0$, with infinite-ranged dipole interactions can be verified by finding the mode dispersion relations for wave vectors along [10], [01], and [11] directions in island coordinates, see Fig. 11. It is found that the ω_∞^- modes along both the [10] and [01] directions go to zero for $q_1 a_1 = \pi$, similar to the behavior in the NN-model, compare Fig. 6, even though the [01] frequency is higher, away from the stabil-

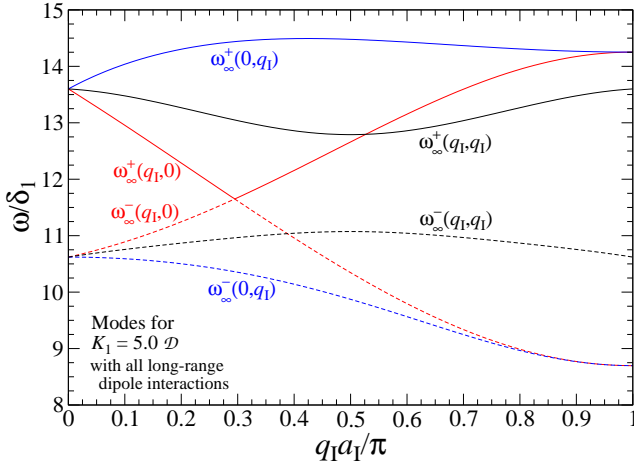


FIG. 12: Dispersion relations using all dipole interactions for a RS at $K_1 = 5.0 \mathcal{D}$, calculated using sums out to $\rho \approx 4000$. While the ω_∞^- and ω_∞^+ frequencies along [01] and [11] island directions are far from each other, they touch or /cross at a point in the [10] direction, i.e., for wave vectors parallel to the RS magnetization.

ity limit point. One concludes that spin waves traveling either parallel to (along [10]) or perpendicular to (along [01]) the magnetic moment of the RS contribute to its instability at weak uniaxial anisotropy in the islands. Even so, very little uniaxial anisotropy is needed to stabilize a RS under the influence of long-range dipole interactions.

Another example of the dispersion relations is shown in Fig. 12 for $K_1 = 5 \mathcal{D}$, $K_3 = 0$. The shapes have changed noticeably from how they appeared at the stability limit for K_1 . Note that the frequencies along [10] touch or cross now at $q_1 a_I \approx 0.3\pi$, while those along [01] and [11] remain very highly separated for all q_I . This is in strong contrast to the result in Fig. 7 for the NN-model above the stability limit. The conclusion is that dipolar interactions are especially influential along the [11] island direction in keeping the higher and lower mode frequencies separated. This effect is highlighted in Fig. 13, where the frequencies along [11] are compared for the NN model (ω_{NN}^\pm), the model with 1st and 2nd nearest neighbors (ω_{2NN}^\pm), and the model with all LRD interactions (ω_∞^\pm). A drastic change occurs when the 2nd nearest neighbors are added, while going from there to very long range interactions shifts the frequencies about 10% higher.

Consider next a real square spin-ice material such as that using Permalloy studied by Wang *et al.* [11], with elongated islands of approximate dimensions $220 \text{ nm} \times 80 \text{ nm} \times 25 \text{ nm}$ thick. Based on the saturation magnetization $M_s = 860 \text{ kA m}^{-1}$ multiplying the volume of elliptical islands, the island magnetic dipole moment was estimated as $\mu = 2.97 \times 10^{-16} \text{ A m}^2$, see Ref. 25. Then supposing a square ice with a close vertex spacing, $a_v = 320 \text{ nm}$ (island NN spacing $a_I = a_v/\sqrt{2}$), the NN dipolar coupling constant in Eq. (3) is $\mathcal{D} = 7.61 \times 10^{-19} \text{ J}$. Simulations in Ref. 28 can be used to estimate the

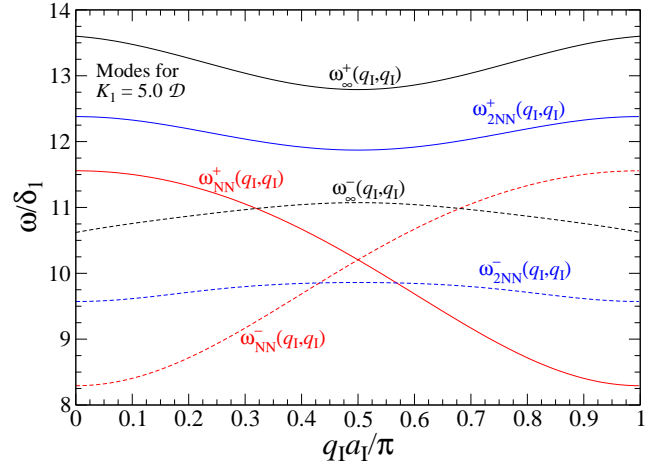


FIG. 13: Dispersion relations at $K_1 = 5.0 \mathcal{D}$, $K_3 = 0$ for wave vectors along the [11] island direction only, comparing the calculations of the NN model (ω_{NN}^\pm), the model with 1st and 2nd nearest neighbors (ω_{2NN}^\pm), and the model with all LRD interactions (ω_∞^\pm).

anisotropy constants, for the chosen island aspect ratios, and they were found [25] to be $K_1 = 2.9 \times 10^{-17} \text{ J}$ and $K_3 = 6.4 \times 10^{-17} \text{ J}$. These are high compared to room temperature thermal energy, which insures stabilization of a remanent or other discrete spin-ice state, and truly forces the oscillations to be of small amplitude. Then the scaled anisotropy parameters needed here are estimated as $K_1 = 38 \mathcal{D}$ and $K_3 = 84 \mathcal{D}$, based on this particular geometry of the island lattice.

For this realistic model, mode frequencies or wave vectors along [10], [01] and [11] directions in island coordinates are plotted in Fig. 14. Relative to the examples with weaker anisotropy, the whole spectrum has been shifted to higher frequencies due to the strong anisotropy in typical spin-ice with greatly elongated islands. Note again the vivid linearity of dispersion relations along the [10] direction near $q_I = 0$, and in the region near the point where higher and lower frequencies touch. The modes along [01], to the contrary, remain widely separated for the whole range of wave vectors. Along [11], both modes ω_∞^+ and ω_∞^- are almost independent of q_I , with only slight variations. The modes along [10] and [01] both approach $q_1 a_I \rightarrow \pi$ with zero slope.

V. CONCLUSIONS

An effective model with Heisenberg-like island dipoles influenced by anisotropies and dipole-dipole interactions has been applied to find the remanent state properties for square spin ice, including the spin configuration, its energy, angular deviation eigenvalues, and the normal modes of oscillation about a RS. The model allows the net dipole of each island to deviate continuously in direction from its long axis, while paying a cost in anisotropy

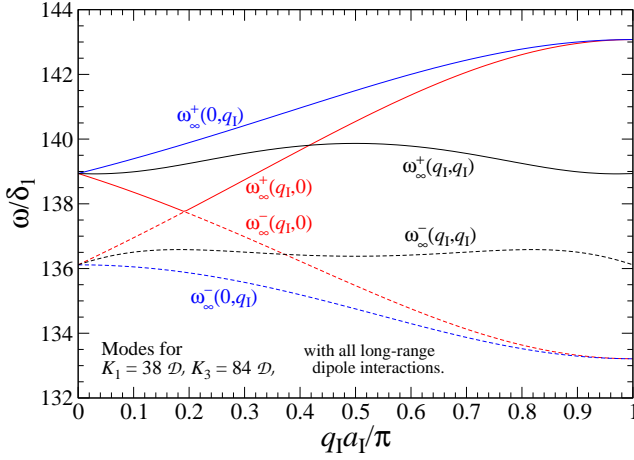


FIG. 14: Dispersion relations in island coordinates using all dipole interactions, for a remanent state at realistic spin-ice parameters appropriate to the square spin-ice of Wang *et al.* [11]. Calculated using sums out to $\rho \approx 4000$. Note the linear dispersions on both sides of the [10] touching point, while the modes stay fairly widely separated along [01] and [11]. Further, the modes along [10] and [01] approach $q_1 a_1 \rightarrow \pi$ with zero slope.

energy. This analysis would not be possible if the island dipoles were represented as Ising spins.

The model with NN-dipole-interactions, although somewhat limited, was used to describe the static and dynamic calculations and to estimate the basic properties. The RS energy (Fig. 3) for $K_1 > K_{1,\min} \approx 2.947 \mathcal{D}$ is $\varepsilon_{\text{NN}} \approx -0.2 \mathcal{D}$, compared to the ground state energy $-3\mathcal{D}$ in the NN-approximation. Hence, the RS exhibits a metastable property. It has considerably higher energy than a ground state but nevertheless is stabilized from small oscillations by relatively weak uniaxial anisotropy of the islands, even when including only NN-dipole-interactions.

In the NN-model, a RS is stable in the absence of planar anisotropy ($K_3 = 0$) as long as the uniaxial anisotropy of an island surpasses $K_{1,\min} = 2.947 \mathcal{D}$, where \mathcal{D} is the NN dipolar interaction strength. The instability for weak uniaxial anisotropy ($K_1 < K_{1,\min}$) can be attributed to in-plane deviation eigenvalues becoming zero at the limiting anisotropy: $\lambda_\phi^+(\pi, 0) \rightarrow 0$ and $\lambda_\phi^-(0, \pi) \rightarrow 0$. The net magnetic moment of the system in the selected remanent state is along the [10] direction of the island lattice ([11] direction of the xy coordinates of the vertex lattice). Although the nonzero magnetization \mathbf{M} breaks the symmetry of the system, modes along island directions [10] and [01] both go unstable at $K_{1,\min}$, see Fig. 6. The eigenvalues λ_ϕ^\pm become imaginary for $K_1 < K_{1,\min}$, implying that large in-plane fluctuations will grow with time for the unstable RS. The out-of-plane deviation eigenvalues λ_θ^\pm remain positive and do not play a role in the instability, even for planar anisotropy $K_3 = 0$, as long as $K_1 > K_{1,\min}$.

A procedure was developed here to include all dipole-

dipole interactions of a central site with neighbors at any distance on the square lattice. With dipole-dipole bonds classified as AA or BB (intrasublattice) and AB (inter-sublattice), it is found that the AA and BB bonds do not change the RS spin angles, but they do affect the dynamic frequencies. LRD interactions cause the sublattice spins to tilt more closely towards each other (closer to the [10] direction) compared to their directions in the NN-model, see Fig. 3. That extra tilting puts the dipoles into an energetically more favorable configuration for dipole-dipole interactions, and lowers the RS energy, while the state remains metastable.

With infinite-range dipole interactions, the instability of the RS for $q_1 a_1 \rightarrow \pi$ still takes place for wave vectors along both the [10] and [01] island directions for $K_1 < K_{1,\min}$, however, the limiting value decreases to $K_{1,\min} = 1.09428 \mathcal{D}$. This implies that the extra dipole interactions beyond NN tend to keep the island spins more strongly along the island axes, with less need for uniaxial anisotropy. A remanent state of square spin ice will not be stable for $K_3 = 0$ unless $K_1 > 1.09428 \mathcal{D}$, a rather weak anisotropy constraint. For the model of a realistic square spin ice, the large anisotropy values $K_1/\mathcal{D} = 38$, $K_3/\mathcal{D} = 84$ very strongly stabilize a remanent state.

The dynamics with LRD interactions is determined by a pair of coupled 2×2 eigenvalue problems, equivalent to a single 4×4 system. Due to the symmetry properties of the involved matrices, the exact frequency eigenvalues of the 4×4 system can be calculated. Generally, the mode frequencies increase as longer range dipole interactions are included. For realistic parameters for square spin-ice, Fig. 14, the mode frequencies are fairly high already due to the islands' anisotropies. The modes ω_∞^\pm with wave vectors along [10] (parallel to the RS magnetization) touch at one point and display a linear behavior at lower wave vectors. The other modes ω_∞^\pm with wave vectors along [01] and [11] stay well separated. Along [11] that mode separation appears to be due to the LRD interactions. These calculations are expected to be applicable for finding state stability and mode properties in other distinct states of spin ice and can be adapted to different lattices.

Appendix A: Full LRD Hamiltonian $H^{(2)}$

Here the quadratic terms in expression (57) for dipole pair energy are fully expanded in the small deviations $\theta_{\mathbf{n}}$ and $\phi_{\mathbf{n}}$ and a complete expression for $H^{(2)}$ that determines the dynamics is given. The quadratic part of an AB pair interaction energy can be written as

$$u_{\text{AB}}^{(2)} = u_{\text{AB}}^{xx} + u_{\text{AB}}^{yy} + u_{\text{AB}}^{xy} + u_{\text{AB}}^{zz}. \quad (\text{A1})$$

Eqs. (58) through (61) are used to get the contributions to $u_{AB}^{(2)}$,

$$\begin{aligned}
u_{AB}^{xx} &= \frac{\mathcal{D}}{4\rho^3} \left(\frac{1}{2} - \frac{3x_I y_I}{\rho^2} \right) \sin 2\phi_A^0 \\
&\quad \times (\phi_n^2 + \phi_m^2 - 2\phi_n \phi_m + \theta_n^2 + \theta_m^2), \\
u_{AB}^{yy} &= \frac{\mathcal{D}}{4\rho^3} \left(\frac{1}{2} + \frac{3x_I y_I}{\rho^2} \right) \sin 2\phi_A^0 \\
&\quad \times (\phi_n^2 + \phi_m^2 - 2\phi_n \phi_m + \theta_n^2 + \theta_m^2), \\
u_{AB}^{xy} &= \frac{3\mathcal{D}}{4\rho^5} (x_I^2 - y_I^2) \\
&\quad \times (\phi_n^2 + \phi_m^2 + 2\phi_n \phi_m + \theta_n^2 + \theta_m^2), \\
u_{AB}^{zz} &= \frac{\mathcal{D}}{\rho^3} \theta_n \theta_m. \tag{A2}
\end{aligned}$$

Then the single AB pair interaction is

$$\begin{aligned}
u_{AB}^{(2)} &= \frac{\mathcal{D}}{\rho^3} \left\{ \frac{1}{4} (\phi_n^2 + \phi_m^2 - 2\phi_n \phi_m + \theta_n^2 + \theta_m^2) \sin 2\phi_A^0 \right. \\
&\quad \left. + \frac{3(x_I^2 - y_I^2)}{4\rho^2} (\phi_n^2 + \phi_m^2 + 2\phi_n \phi_m + \theta_n^2 + \theta_m^2) + \theta_n \theta_m \right\}. \tag{A3}
\end{aligned}$$

This is summed over all AB pairs, which is one contribution to $H^{(2)}$. Each pair must be summed only once, which can be done by restricting \mathbf{n} to be an A-site only and \mathbf{m} to be a B-site only, denoted as

$$U_{AB}^{(2)} = \sum_{\mathbf{n}}^A \sum_{\mathbf{m}}^B u_{AB}^{(2)}. \tag{A4}$$

But the expressions are symmetric in \mathbf{n} and \mathbf{m} , so that summing ϕ_m^2 over *all* \mathbf{m} is equivalent to summing ϕ_n^2 over *all* \mathbf{n} . That means ϕ_m^2 can be removed, and \mathbf{n} can be summed over all sites of both sublattices. The term θ_m^2 can be removed for the same reason. For the cross terms, let $\mathbf{m} = \mathbf{n} + \mathbf{r}$, sum over the allowed AB displacements \mathbf{r} , sum over *all* \mathbf{n} , and then divide by two to undo the double counting of bonds. \mathbf{n} might be an A or B site, it doesn't matter, as long as $\mathbf{r} = (x_I, y_I)$ is an AB bond, which is enforced with $(x_I + y_I)$ being an odd integer. This gives the AB bond contribution to $H^{(2)}$,

$$\begin{aligned}
U_{AB}^{(2)} &= \sum_{\mathbf{n}} \sum_{\mathbf{r}}^{\text{AB}} \frac{\mathcal{D}}{\rho^3} \left\{ \frac{1}{4} (\phi_n^2 - \phi_n \phi_{\mathbf{n}+\mathbf{r}} + \theta_n^2) \sin 2\phi_A^0 \right. \\
&\quad \left. + \frac{3(x_I^2 - y_I^2)}{4\rho^2} (\phi_n^2 + \phi_n \phi_{\mathbf{n}+\mathbf{r}} + \theta_n^2) + \frac{1}{2} \theta_n \theta_{\mathbf{m}} \right\}. \tag{A5}
\end{aligned}$$

A similar procedure is applied for AA bonds. Eqs. (62)

through (64) give

$$\begin{aligned}
u_{AA}^{xx} &= \frac{\mathcal{D}}{2\rho^3} \left(\frac{1}{2} - \frac{3x_I y_I}{\rho^2} \right) \\
&\quad \times [(\phi_n^2 + \phi_m^2 + \theta_n^2 + \theta_m^2) \cos^2 \phi_A^0 - 2\phi_n \phi_m \sin^2 \phi_A^0], \\
u_{AA}^{yy} &= \frac{\mathcal{D}}{2\rho^3} \left(\frac{1}{2} + \frac{3x_I y_I}{\rho^2} \right) \\
&\quad \times [(\phi_n^2 + \phi_m^2 + \theta_n^2 + \theta_m^2) \sin^2 \phi_A^0 - 2\phi_n \phi_m \cos^2 \phi_A^0], \\
u_{AA}^{xy} &= \frac{3\mathcal{D}}{4\rho^5} (x_I^2 - y_I^2) \\
&\quad \times (\phi_n^2 + \phi_m^2 + 2\phi_n \phi_m + \theta_n^2 + \theta_m^2) \sin 2\phi_A^0, \\
u_{AA}^{zz} &= \frac{\mathcal{D}}{\rho^3} \theta_n \theta_m. \tag{A6}
\end{aligned}$$

Their sum is a single AA pair interaction,

$$\begin{aligned}
u_{AA}^{(2)} &= \frac{\mathcal{D}}{\rho^3} \left\{ \frac{1}{4} (\phi_n^2 + \phi_m^2 - 2\phi_n \phi_m + \theta_n^2 + \theta_m^2) + \theta_n \theta_m \right. \\
&\quad \left. + \frac{3(x_I^2 - y_I^2)}{4\rho^2} (\phi_n^2 + \phi_m^2 + 2\phi_n \phi_m + \theta_n^2 + \theta_m^2) \sin 2\phi_A^0 \right. \\
&\quad \left. - \frac{3x_I y_I}{2\rho^2} (\phi_n^2 + \phi_m^2 + 2\phi_n \phi_m + \theta_n^2 + \theta_m^2) \cos 2\phi_A^0 \right\}. \tag{A7}
\end{aligned}$$

When $u_{AA}^{(2)}$ is summed over all AA pairs, this gives another contribution to $H^{(2)}$. In this case both \mathbf{n} and \mathbf{m} must be selected from the A-sites, and the sum is

$$U_{AA}^{(2)} = \frac{1}{2} \sum_{\mathbf{n}}^A \sum_{\mathbf{m} \neq \mathbf{n}}^A u_{AA}^{(2)}. \tag{A8}$$

where $\frac{1}{2}$ undoes the double counting of AA bonds. But summing ϕ_m^2 over all A-sites gives the same as summing ϕ_n^2 over all A-sites. Therefore this can be written indicating that \mathbf{n} is an A-site while the displacements $\mathbf{r} = (x_I, y_I)$ must be AA bonds, enforced by $(x_I + y_I)$ being even integers. This gives

$$\begin{aligned}
U_{AA}^{(2)} &= \sum_{\mathbf{n}}^A \sum_{\mathbf{r}}^{\text{AA}} \frac{\mathcal{D}}{\rho^3} \left\{ \frac{1}{4} (\phi_n^2 - \phi_n \phi_{\mathbf{n}+\mathbf{r}} + \theta_n^2) + \frac{1}{2} \theta_n \theta_m \right. \\
&\quad \left. + \frac{3(x_I^2 - y_I^2)}{4\rho^2} (\phi_n^2 + \phi_n \phi_{\mathbf{n}+\mathbf{r}} + \theta_n^2) \sin 2\phi_A^0 \right. \\
&\quad \left. - \frac{3x_I y_I}{2\rho^2} (\phi_n^2 + \phi_n \phi_{\mathbf{n}+\mathbf{r}} + \theta_n^2) \cos 2\phi_A^0 \right\}. \tag{A9}
\end{aligned}$$

Finally there are BB bonds, very similar to AA bonds, however, the terms differ because the equilibrium dipole directions on the two sublattices are different. Eqs. (65)

through (67) give

$$\begin{aligned}
u_{\text{BB}}^{xx} &= \frac{\mathcal{D}}{2\rho^3} \left(\frac{1}{2} - \frac{3x_1 y_1}{\rho^2} \right) \\
&\times [(\phi_{\mathbf{n}}^2 + \phi_{\mathbf{m}}^2 + \theta_{\mathbf{n}}^2 + \theta_{\mathbf{m}}^2) \sin^2 \phi_A^0 - 2\phi_{\mathbf{n}} \phi_{\mathbf{m}} \cos^2 \phi_A^0], \\
u_{\text{BB}}^{yy} &= \frac{\mathcal{D}}{2\rho^3} \left(\frac{1}{2} + \frac{3x_1 y_1}{\rho^2} \right) \\
&\times [(\phi_{\mathbf{n}}^2 + \phi_{\mathbf{m}}^2 + \theta_{\mathbf{n}}^2 + \theta_{\mathbf{m}}^2) \cos^2 \phi_A^0 - 2\phi_{\mathbf{n}} \phi_{\mathbf{m}} \sin^2 \phi_A^0], \\
u_{\text{BB}}^{xy} &= \frac{3\mathcal{D}}{4\rho^5} (x_1^2 - y_1^2) \\
&\times (\phi_{\mathbf{n}}^2 + \phi_{\mathbf{m}}^2 + 2\phi_{\mathbf{n}} \phi_{\mathbf{m}} + \theta_{\mathbf{n}}^2 + \theta_{\mathbf{m}}^2) \sin 2\phi_A^0, \\
u_{\text{BB}}^{zz} &= \frac{\mathcal{D}}{\rho^3} \theta_{\mathbf{n}} \theta_{\mathbf{m}}. \tag{A10}
\end{aligned}$$

The displacements that connect BB pairs are the same as for AA pairs, selecting $\mathbf{r} = (x_1, y_1)$ with $(x_1 + y_1)$ being even integers. Summing appropriately over all the BB pairs gives their contribution to $H^{(2)}$,

$$\begin{aligned}
U_{\text{BB}}^{(2)} &= \sum_{\mathbf{n}} \sum_{\mathbf{r}}^{\text{BB}} \frac{\mathcal{D}}{\rho^3} \left\{ \frac{1}{4} (\phi_{\mathbf{n}}^2 - \phi_{\mathbf{n}} \phi_{\mathbf{n}+\mathbf{r}} + \theta_{\mathbf{n}}^2) + \frac{1}{2} \theta_{\mathbf{n}} \theta_{\mathbf{m}} \right. \\
&+ \frac{3(x_1^2 - y_1^2)}{4\rho^2} (\phi_{\mathbf{n}}^2 + \phi_{\mathbf{n}} \phi_{\mathbf{n}+\mathbf{r}} + \theta_{\mathbf{n}}^2) \sin 2\phi_A^0 \\
&\left. + \frac{3x_1 y_1}{2\rho^2} (\phi_{\mathbf{n}}^2 + \phi_{\mathbf{n}} \phi_{\mathbf{n}+\mathbf{r}} + \theta_{\mathbf{n}}^2) \cos 2\phi_A^0 \right\}. \tag{A11}
\end{aligned}$$

The term with $x_1 y_1$ is reversed in sign from that in $U_{\text{AA}}^{(2)}$, Eq. (A9), which is obtained more easily by transforming $\phi_A^0 \rightarrow \frac{\pi}{2} - \phi_A^0$ in going from AA interactions to BB interactions for the same \mathbf{r} .

The final contribution to $H^{(2)}$ comes from the islands' anisotropies, whose quadratic contribution can be obtained from (17),

$$U_K^{(2)} = \sum_{\mathbf{n}} [(K_1 \cos 2\phi_A^0) \phi_{\mathbf{n}}^2 + (K_1 \cos^2 \phi_A^0 + K_3) \theta_{\mathbf{n}}^2]. \tag{A12}$$

Then the total second order Hamiltonian is the sum of all these parts,

$$H^{(2)} = U_K^{(2)} + U_{\text{AB}}^{(2)} + U_{\text{AA}}^{(2)} + U_{\text{BB}}^{(2)}. \tag{A13}$$

Appendix B: Matrix elements of $H^{(2)}$

The matrix elements needed in the dynamics calculations can be found from the full quadratic Hamiltonian $H^{(2)}$, using its quadratic form,

$$H^{(2)} = \frac{1}{2} \psi_{\theta}^{\dagger} \mathbf{M}_{\theta} \psi_{\theta} + \frac{1}{2} \psi_{\phi}^{\dagger} \mathbf{M}_{\phi} \psi_{\phi}. \tag{B1}$$

This is equivalent to a double sum over all \mathbf{n} and \mathbf{m} ,

$$H^{(2)} = \frac{1}{2} \sum_{\mathbf{n}, \mathbf{m}} (M_{\theta, \mathbf{n}, \mathbf{m}} \theta_{\mathbf{n}} \theta_{\mathbf{m}} + M_{\phi, \mathbf{n}, \mathbf{m}} \phi_{\mathbf{n}} \phi_{\mathbf{m}}). \tag{B2}$$

The matrix elements can be found either by inspection of $H^{(2)}$ in (A13) or by second derivatives,

$$M_{\theta, \mathbf{n}, \mathbf{m}} = \frac{\partial^2 H^{(2)}}{\partial \theta_{\mathbf{n}} \partial \theta_{\mathbf{m}}}, \quad M_{\phi, \mathbf{n}, \mathbf{m}} = \frac{\partial^2 H^{(2)}}{\partial \phi_{\mathbf{n}} \partial \phi_{\mathbf{m}}}. \tag{B3}$$

The factors $\theta_{\mathbf{n}}^2$ and $\phi_{\mathbf{n}}^2$ appear in all four parts of $H^{(2)}$, so all LRD interactions contribute to on-site ($M_{\mathbf{n}, \mathbf{n}}$) couplings. Those matrix elements are

$$\begin{aligned}
M_{\theta, \mathbf{n}, \mathbf{n}} &= M_{\text{dd}} + 2(K_1 \cos^2 \phi_A^0 + K_3), \\
M_{\phi, \mathbf{n}, \mathbf{n}} &= M_{\text{dd}} + 2K_1 \cos 2\phi_A^0, \tag{B4}
\end{aligned}$$

where M_{dd} is the LRD part, the same for θ and ϕ ,

$$\begin{aligned}
M_{\text{dd}} &= \sum_{\mathbf{r}}^{\text{AB}} \frac{\mathcal{D}}{\rho^3} \left[\frac{1}{2} \sin 2\phi_A^0 + \frac{3(x_1^2 - y_1^2)}{2\rho^2} \right] \\
&+ \sum_{\mathbf{r}}^{\text{AA}} \frac{\mathcal{D}}{\rho^3} \left[\frac{1}{2} + \frac{3(x_1^2 - y_1^2)}{2\rho^2} \sin 2\phi_A^0 \mp \frac{3x_1 y_1}{2\rho^2} \cos 2\phi_A^0 \right]. \tag{B5}
\end{aligned}$$

For A-sites (B-sites), the last term takes the minus (plus) sign. For an infinite system, however, the sums involving x_1 and y_1 are zero due to symmetry. M_{dd} is the same for A- and B-sites, and depends on sums over $1/\rho^3$ for AB or AA bonds,

$$M_{\text{dd}} = \frac{1}{2} \mathcal{D} (s_{\text{AB}} \sin 2\phi_A^0 + s_{\text{AA}}) \tag{B6}$$

where s_{AB} and s_{AA} were defined in (70). Note that $-\frac{1}{2} M_{\text{dd}}$ already appears in the expression (71) for equilibrium energy per island, $H^{(0)}/N$.

There are also matrix elements connecting different sites, which can be grouped according to bond type (AB, AA or BB), and depend on the bond displacement $\mathbf{r} = (x_1, y_1)$ or on the distance $\rho = \sqrt{x_1^2 + y_1^2}$. For the θ coordinate, they don't depend on the bond type:

$$M_{\theta, \mathbf{n}, \mathbf{n}+\mathbf{r}}^{\text{AB}} = M_{\theta, \mathbf{n}, \mathbf{n}+\mathbf{r}}^{\text{AA}} = M_{\theta, \mathbf{n}, \mathbf{n}+\mathbf{r}}^{\text{BB}} = \frac{\mathcal{D}}{\rho^3}. \tag{B7}$$

For the ϕ coordinate, the bond type is important:

$$\begin{aligned}
M_{\phi, \mathbf{n}, \mathbf{n}+\mathbf{r}}^{\text{AB}} &= \frac{\mathcal{D}}{\rho^3} \left[-\frac{1}{2} \sin 2\phi_A^0 + \frac{3(x_1^2 - y_1^2)}{2\rho^2} \right], \tag{B8} \\
M_{\phi, \mathbf{n}, \mathbf{n}+\mathbf{r}}^{\text{AA}} &= \frac{\mathcal{D}}{\rho^3} \left[-\frac{1}{2} + \frac{3(x_1^2 - y_1^2)}{2\rho^2} \sin 2\phi_A^0 - \frac{3x_1 y_1}{\rho^2} \cos 2\phi_A^0 \right], \\
M_{\phi, \mathbf{n}, \mathbf{n}+\mathbf{r}}^{\text{BB}} &= \frac{\mathcal{D}}{\rho^3} \left[-\frac{1}{2} + \frac{3(x_1^2 - y_1^2)}{2\rho^2} \sin 2\phi_A^0 + \frac{3x_1 y_1}{\rho^2} \cos 2\phi_A^0 \right].
\end{aligned}$$

None of the above matrix elements depend on the site \mathbf{n} , but only on the displacement from \mathbf{n} to $\mathbf{n}+\mathbf{r}$, where $\mathbf{r} = (x_1, y_1)$ in integer island coordinates.

1. Elements of the dynamic matrices \mathbf{m} and \mathbf{n}

The elements of the dynamic matrices \mathbf{m} (which acts on a θ wave function) and \mathbf{n} (which acts on a ϕ wave

function) with all LRD interactions are implicitly defined via Eq. (74), with traveling waves inserted. The aa and bb elements stay within a sublattice, so they involve Fourier sums over $M_{\mathbf{n},\mathbf{n}+\mathbf{r}}^{\text{AA}}$ and $M_{\mathbf{n},\mathbf{n}+\mathbf{r}}^{\text{BB}}$. For the θ operator \mathbf{m} ,

$$\begin{aligned} m_{aa} = m_{bb} &= \frac{\gamma_e}{\mu} \left(M_{\theta,\mathbf{n},\mathbf{n}} + \sum_{\mathbf{r}}^{\text{AA}} M_{\theta,\mathbf{n},\mathbf{n}+\mathbf{r}}^{\text{AA}} e^{i\mathbf{q}\cdot\mathbf{r}} \right) \\ &= \frac{\gamma_e}{\mu} [M_{\theta,\mathbf{n},\mathbf{n}} + \mathcal{D}f_{\text{evn}}(\mathbf{q})]. \end{aligned} \quad (\text{B9})$$

This depends on a Fourier sum over AA displacements,

$$f_{\text{evn}}(\mathbf{q}) \equiv \sum_{\mathbf{r}}^{\text{AA}} \frac{e^{i\mathbf{q}\cdot\mathbf{r}}}{\rho^3} = \sum_{x_1+y_1}^{\text{even}} \frac{\cos[(q_{x_1}x_1 + q_{y_1}y_1)a_1]}{(x_1^2 + y_1^2)^{3/2}}. \quad (\text{B10})$$

For the ϕ operator \mathbf{n} , the corresponding matrix elements are

$$\begin{aligned} n_{aa} &= \frac{\gamma_e}{\mu} \left(M_{\phi,\mathbf{n},\mathbf{n}} + \sum_{\mathbf{r}}^{\text{AA}} M_{\phi,\mathbf{n},\mathbf{n}+\mathbf{r}}^{\text{AA}} e^{i\mathbf{q}\cdot\mathbf{r}} \right) = \frac{\gamma_e}{\mu} \left\{ M_{\phi,\mathbf{n},\mathbf{n}} + \mathcal{D} \left[\frac{3}{2}d_{\text{evn}}(\mathbf{q}) \sin 2\phi_A^0 - 3f_{\text{evn}}^{xy}(\mathbf{q}) \cos 2\phi_A^0 - \frac{1}{2}f_{\text{evn}}(\mathbf{q}) \right] \right\}. \\ n_{bb} &= \frac{\gamma_e}{\mu} \left(M_{\phi,\mathbf{n},\mathbf{n}} + \sum_{\mathbf{r}}^{\text{BB}} M_{\phi,\mathbf{n},\mathbf{n}+\mathbf{r}}^{\text{BB}} e^{i\mathbf{q}\cdot\mathbf{r}} \right) = \frac{\gamma_e}{\mu} \left\{ M_{\phi,\mathbf{n},\mathbf{n}} + \mathcal{D} \left[\frac{3}{2}d_{\text{evn}}(\mathbf{q}) \sin 2\phi_A^0 + 3f_{\text{evn}}^{xy}(\mathbf{q}) \cos 2\phi_A^0 - \frac{1}{2}f_{\text{evn}}(\mathbf{q}) \right] \right\}. \\ n_{ab} = n_{ba} &= \frac{\gamma_e}{\mu} \sum_{\mathbf{r}}^{\text{AB}} M_{\phi,\mathbf{n},\mathbf{n}+\mathbf{r}}^{\text{AB}} e^{i\mathbf{q}\cdot\mathbf{r}} = \frac{\gamma_e}{\mu} \mathcal{D} \left[\frac{3}{2}d_{\text{odd}}(\mathbf{q}) - \frac{1}{2}f_{\text{odd}}(\mathbf{q}) \sin 2\phi_A^0 \right]. \end{aligned} \quad (\text{B13})$$

These depend on $f_e(\mathbf{q})$ and $f_o(\mathbf{q})$ and other Fourier sums,

$$\begin{aligned} f_{\text{evn}}^{xy}(\mathbf{q}) &\equiv \sum_{x_1+y_1}^{\text{even}} \frac{x_1y_1 \cos[(q_{x_1}x_1 + q_{y_1}y_1)a_1]}{(x_1^2 + y_1^2)^{5/2}}, \\ d_{\text{evn}}(\mathbf{q}) &\equiv \sum_{x_1+y_1}^{\text{even}} \frac{(x_1^2 - y_1^2) \cos[(q_{x_1}x_1 + q_{y_1}y_1)a_1]}{(x_1^2 + y_1^2)^{5/2}}, \\ d_{\text{odd}}(\mathbf{q}) &\equiv \sum_{x_1+y_1}^{\text{odd}} \frac{(x_1^2 - y_1^2) \cos[(q_{x_1}x_1 + q_{y_1}y_1)a_1]}{(x_1^2 + y_1^2)^{5/2}}. \end{aligned} \quad (\text{B14})$$

Appendix C: Eigenvalues of the 4×4 dynamic matrix

The general dynamic equation (77) has the expanded expression,

$$\begin{bmatrix} 0 & 0 & m_{aa} & m_{ab} \\ 0 & 0 & m_{ba} & m_{bb} \\ n_{aa} & n_{ab} & 0 & 0 \\ n_{ba} & n_{bb} & 0 & 0 \end{bmatrix} \begin{bmatrix} a_\phi \\ b_\phi \\ ia_\theta \\ ib_\theta \end{bmatrix} = \omega \begin{bmatrix} a_\phi \\ b_\phi \\ ia_\theta \\ ib_\theta \end{bmatrix}. \quad (\text{C1})$$

This is $\mathbf{W}\psi = \omega\psi$, where \mathbf{W} is the 4×4 matrix. The solution requires the determinant $D(\omega) = |\mathbf{W} - \omega\mathbf{I}|$ to

The restriction that $x_1 + y_1$ is even keeps the bonds on the same sublattice. The ab and ba elements are determined by Fourier sums over $M_{\mathbf{n},\mathbf{n}+\mathbf{r}}^{\text{AB}}$,

$$m_{ab} = m_{ba} = \frac{\gamma_e}{\mu} \sum_{\mathbf{r}}^{\text{AB}} M_{\theta,\mathbf{n},\mathbf{n}+\mathbf{r}}^{\text{AB}} e^{i\mathbf{q}\cdot\mathbf{r}} = \frac{\gamma_e}{\mu} \mathcal{D}f_{\text{odd}}(\mathbf{q}), \quad (\text{B11})$$

where the sum is restricted by $x_1 + y_1$ being odd,

$$f_{\text{odd}}(\mathbf{q}) \equiv \sum_{\mathbf{r}}^{\text{AB}} \frac{e^{i\mathbf{q}\cdot\mathbf{r}}}{\rho^3} = \sum_{x_1+y_1}^{\text{odd}} \frac{\cos[(q_{x_1}x_1 + q_{y_1}y_1)a_1]}{(x_1^2 + y_1^2)^{3/2}}. \quad (\text{B12})$$

be zero. This is

$$D(\omega) = \begin{vmatrix} -\omega & 0 & m_{aa} & m_{ab} \\ 0 & -\omega & m_{ba} & m_{bb} \\ n_{aa} & n_{ab} & -\omega & 0 \\ n_{ba} & n_{bb} & 0 & -\omega \end{vmatrix} = 0. \quad (\text{C2})$$

Evaluating $D(\omega)$ by the first row, the first term is

$$\begin{aligned} D_1(\omega) &= -\omega \begin{vmatrix} -\omega & m_{ba} & m_{bb} \\ n_{ab} & -\omega & 0 \\ n_{bb} & 0 & -\omega \end{vmatrix} \\ &= -\omega [-\omega^3 + (m_{ba}n_{ab} + m_{bb}n_{bb})\omega]. \end{aligned} \quad (\text{C3})$$

The next term is

$$\begin{aligned} D_2(\omega) &= m_{aa} \begin{vmatrix} 0 & -\omega & m_{bb} \\ n_{aa} & n_{ab} & 0 \\ n_{ba} & n_{bb} & -\omega \end{vmatrix} \\ &= m_{aa} [-n_{aa}\omega^2 + m_{bb}(n_{aa}n_{bb} - n_{ab}n_{ba})]. \end{aligned} \quad (\text{C4})$$

The third and last term is

$$\begin{aligned} D_3(\omega) &= -m_{ab} \begin{vmatrix} 0 & -\omega & m_{ba} \\ n_{aa} & n_{ab} & -\omega \\ n_{ba} & n_{bb} & 0 \end{vmatrix} \\ &= -m_{ab} [n_{ba}\omega^2 + m_{ba}(n_{aa}n_{bb} - n_{ab}n_{ba})]. \end{aligned} \quad (\text{C5})$$

The total determinant is the sum, $D(\omega) = D_1 + D_2 + D_3$, which is quadratic in ω^2 ,

$$D(\omega) = \omega^4 - [m_{aa}n_{aa} + m_{bb}n_{bb} + m_{ab}n_{ba} + m_{ba}n_{ab}]\omega^2 + (m_{aa}m_{bb} - m_{ab}m_{ba})(n_{aa}n_{bb} - n_{ab}n_{ba}) = 0. \quad (C6)$$

That is very general, and it is the same as

$$D(\omega) = \omega^4 - (\mathbf{m}^T \cdot \mathbf{n}) \omega^2 + |\mathbf{m}||\mathbf{n}| = 0. \quad (C7)$$

That involves a scalar product of the 2×2 matrices and their determinants. Then the eigenvalues in this rather

general case are determined by the quadratic formula,

$$\omega^2 = \frac{1}{2} \left[(\mathbf{m}^T \cdot \mathbf{n}) \pm \sqrt{(\mathbf{m}^T \cdot \mathbf{n})^2 - 4|\mathbf{m}||\mathbf{n}|} \right]. \quad (C8)$$

One can verify that all four eigenvalues are real, and they come in $+/-$ pairs, corresponding to opposite directions of propagation. The \pm in the expression gives two fundamental solutions (higher and lower frequencies), whose dispersion relations are denoted $\omega_{\infty}^+(\mathbf{q})$ and $\omega_{\infty}^-(\mathbf{q})$, where the ∞ subscript indicates that all LRD interactions are included.

-
- [1] S. H. Skjærvø, C.H. Marrows, R.L. Stamps and L.J. Heyderman, *Nat. Rev. Phys.* **2**, 13 (2020).
- [2] C. Nisoli, R. Moessner and P. Schiffer, *Rev. Mod. Phys.* **85** 1473 (2013).
- [3] V.D. Nguyen, Y. Perrin, S. Le Denmat, B. Canals, and N. Rougemaille, *Phys. Rev. B* **96** 014402 (2017).
- [4] J.P. Morgan, A. Stein, S. Langridge and C. Marrows, *Nature Phys.* **7** 75 (2011).
- [5] R.C. Silva, F.S. Nascimento, L.A. S. Mól, W.A. Moura-Melo, and A.R. Pereira, *New J. Phys.* **14**, 015008 (2012).
- [6] I.R.B. Ribeiro, F.S. Nascimento, S.O. Ferreira, W.A. Moura-Melo, C.A.R. Costa, J. Borme, P.P. Freitas, G.M. Wysin, C.I.L. de Araujo and A.R. Pereira *Scientific Reports* **7**, 13982 (2017).
- [7] C. Nisoli, in *The Role of Topology in Materials*, pp 85–112, S. Gupta and A. Saxena (eds), Springer Series in Solid-State Sciences, vol 189. Springer, Cham. (2018), https://doi.org/10.1007/978-3-319-76596-9_4
- [8] G. Möller and R. Moessner *Phys. Rev. Lett.* **96**, 237202 (2006).
- [9] G. Möller and R. Moessner, *Phys. Rev. B* **80**, 140409(R) (2009).
- [10] L.A.S. Mól, R.L. Silva, R.C. Silva, A.R. Pereira, W.A. Moura-Melo, and B.V. Costa, *J. Appl. Phys.* **106**, 063913 (2009).
- [11] R.F. Wang, C. Nisoli, R.S. Freitas, J. Li, W. McConville, B.J. Cooley, M.S. Lund, N. Samarth, C. Leighton, V.H. Crespi, and P. Schiffer, *Nature* **439** 303 (2006).
- [12] X. Ke, J. Li, C. Nisoli, Paul E. Lammert, W. McConville, R.F. Wang, V.H. Crespi, and P. Schiffer, *Phys. Rev. Lett.* **101** 037205 (2008).
- [13] C. Nisoli, J. Li, X. Ke, D. Garand, P. Schiffer, and V.H. Crespi, *Phys. Rev. Lett.* **105**, 047205 (2010).
- [14] J.M. Porro, A. Bedoya-Pinto, A. Berger, and P. Vavasori, *New J. Phys.* **15**, 055012 (2013).
- [15] A. Farhan, P.M. Derlet, A. Kleibert, A. Balan, R.V. Chopdekar, M. Wyss, J. Perron, A. Scholl, F. Noltling, and L.J. Heyderman, *Phys. Rev. Lett.* **111**, 057204 (2013).
- [16] X. Zhang, Y. Lao, J. Sklenar, N.S. Bingham, J.T. Batley, J.D. Watts, C. Nisoli, C. Leighton, and P. Schiffer, *APL Materials* **7** 111112 (2019).
- [17] Vassilios Kapaklis, Unnar B Arnalds, Adam Harman-Clarke, Evangelos Th Papaioannou, Masoud Karimipour, Panagiotis Korelis, Andrea Taroni, Peter C W Holdsworth, Steven T Bramwell and Björgvin Hjörvarsson, *New Journal of Physics* **14**, 035009 (2012).
- [18] S. Gliga, A. Kákay, R. Hertel, and O.G. Heinonen *Phys. Rev. Lett.* **110** 117205 (2013).
- [19] M.B. Jungfleisch, W. Zhang, E. Iacocca, J. Sklenar, J. Ding, W. Jiang, S. Zhang, J.E. Pearson, V. Novosad, J.B. Ketterson, O. Heinonen, and A. Hoffmann, *Phys. Rev. B* **93** 100401(R) (2016).
- [20] E. Iacocca, S. Gliga, R.L. Stamps, and O. Heinonen, *Phys. Rev. B* **93** 134420 (2016).
- [21] D.M. Arroyo, J.C. Gartside, and W.R. Branford, *Phys. Rev. B* **100** 214425 (2019).
- [22] T.D. Lasnier and G.M. Wysin *Phys. Rev. B* **101** 224428 (2020).
- [23] N. Arora and P Das, *AIP Advances* **11** 035030 (2021).
- [24] W. Heisenberg *Z. Phys.* **49** 619 (1928).
- [25] G.M. Wysin, W.A. Moura-Melo, L.A.S. Mól, and A.R. Pereira *New J. Phys.* **15** 045029 (2013).
- [26] E. Ising *Z. Physik* **31** 253 (1925).
- [27] E. Östman, U.B. Arnalds, V. Kapaklis, A. Taroni, and B. Hjörvarsson *J. Phys.: Condens. Matter* **30** 365301 (2018).
- [28] G.M. Wysin, W.A. Moura-Melo, L.A.S. Mól, and A.R. Pereira *J. Phys.: Condens. Matter* **24** 296001 (2012).
- [29] O. Brunn, Y. Perrin, B. Canals, and N. Rougemaille *Phys. Rev. B* **103** 094405 (2021).
- [30] G.M. Wysin, *J. Phys.: Condens. Matter* **34** 065803 (2021).
- [31] G.M. Wysin, A.R. Pereira, W.A. Moura-Melo, and C.I.L. de Araujo *J. Phys.: Condens. Matter* **27** 076004 (2015).
- [32] N. Rougemaille, F. Montaigne, B. Canals, A. Duluard, D. Lacour, M. Hehn, R. Belkhou, O. Fruchart, S. El Mousaoui, A. Bendounan, and F. Maccherozzi, *Phys. Rev. Lett.* **106**, 057209 (2011).
- [33] Y. Shevchenko, A. Makarov, and K. Nefedev *Phys. Lett. A* **381(5)** 428-434 (2017).
- [34] David Jiles, *Introduction to Magnetism and Magnetic Materials*, Ch. 11, (London: Chapman and Hall 1991).
- [35] G.M. Wysin *Magnetic Excitations & Geometric Confinement: Theory and Simulations*, Ch. 2, (London: IOP Expanding Physics ebook 2015)